Epigenetic coordination of transcriptional and translational programs in hypoxia

Kathleen Watt[1]*, Bianca Dauber[2]*, Krzysztof J Szkop[1]*, Laura Lee[3], Predrag Jovanovic[4,5], Shan Chen[1], Laìa Masvidal[1], Kristofersson Tandoc[4,5], Ranveer Palia[4,5], Ivan Topisirovic[4,5,6], Ola Larsson[1]**, Lynne-Marie Postovit[2,3]**

[1]Department of Oncology-Pathology, Science for Life Laboratory, Karolinska Institutet, Stockholm, Sweden.
[2]Department of Biomedical and Molecular Sciences, Queen's University, Kingston, ON, Canada.
[3]Department of Oncology, University of Alberta, Edmonton, AB, Canada.
[4]Lady Davis Institute, Sir Mortimer B. Davis Jewish General Hospital, Montréal, QC, Canada.
[5]Division of Experimental Medicine McGill University, Montréal, QC, Canada.
[6]Gerald Bronfman Department of Oncology, and Department of Biochemistry McGill University, Montréal, QC, Canada.
*equally contributing authors; ** co-corresponding authors.

SUMMARY

Adaptation to stresses entails coordination of transcriptional and post-transcriptional gene regulation, but the mechanisms remain largely unknown. We interrogated the effects of hypoxia on transcriptomes, epigenomes and translatomes of T47D breast cancer cells and H9 human embryonic stem cells. This revealed hypoxia-induced alterations in H3K4me3 associating with pervasive changes in transcription start site (TSS) selection, leading to 5'UTR remodeling and a concomitant reshaping of translational landscapes. Importantly, this epigenetically driven reprogramming of translation is distinct from HIF1-dependent transcriptional mechanisms, and TSS switching appears to occur independently of alterations in transcript abundance. While TSS switching is coordinated with the integrated stress response (ISR) and mTOR-guided translational reprogramming, it also acts independently to regulate translation in hypoxia. Moreover, comparable TSS switching was observed following H3K4me3 accumulation in the absence of hypoxia, pinpointing H3K4me3 as underlying TSS selection. These results demonstrate a previously unappreciated mechanism of translational regulation driven by epigenetic reprogramming of the 5'UTRome, which is orchestrated with other hypoxia-triggered adaptive mechanisms.

INTRODUCTION

Cellular plasticity (the ability to adapt in response to changes in microenvironment) is fundamental to cancer cell survival and metastasis in essentially all solid tumors[1]. Hypoxia is a major microenvironmental factor to which cancer cells must be able to adapt, and has been shown to enhance plasticity and enrich for cancer stem-cell-like phenotypes[1,2]. Cellular plasticity enables the reprogramming of gene expression at transcriptional and post-transcriptional levels, thereby facilitating the rapid and dynamic regulation of the proteome in response to changing microenvironments[3]. A hypoxic milieu imposes metabolic restrictions that impact various mechanisms regulating gene expression[4,5]. For instance, emerging data indicate that restriction of oxygen and subsequent perturbations in metabolites dramatically alter the epigenome[6,7]. To this end, covalent modifications of histones can activate or suppress transcription in a dynamic and context-dependent manner[8]. Trimethylation of lysine 4 of the histone H3 subunit (H3K4me3) occurs around transcription start sites (TSSs), where it has been reported to correlate with both the degree and consistency of transcriptional activation[8,9,10,11]. H3K4 methylation is deposited by SET and SET-like domain-containing methyltransferase complexes and erased by Jumonji C (JMJC) histone demethylases such as histone lysine demethylase 5 (KDM5)[12]. A number of JMJC histone demethylases were identified as direct transcriptional targets of HIF1□, with increased transcript and protein levels in conditions where HIF1□ is stabilized[13,14,15]. However, due to these enzymes being □-ketoglutarate-dependent dioxygenases, this upregulation is counteracted by reduced activity when O_2 is limiting[16], resulting in the accumulation of H3K4 methylation under hypoxia and thereby chromatin remodeling and enhanced cellular plasticity[7,6]. However, the effect of this oxygen-sensing capacity of chromatin on processes such as TSS selection has not yet been considered.

Due to the high energy demands of protein synthesis[17], under hypoxia when energy is limiting, cells undergo a global decrease in mRNA translation[5,3]. This occurs through inhibition of mammalian/mechanistic Target of Rapamycin (mTOR) signaling[18], which prevents assembly of the eIF4F complex formation and inhibits LARP1 to limit cap-dependent translation initiation, and via activation of the integrated stress response (ISR) whereby eIF2α phosphorylation-dependent suppression of eIF2B decreases ternary complex recycling required for initiator tRNA delivery[5,19]. Against the backdrop of reduced global protein synthesis, selective translation of mRNAs encoding central regulators of stress responses is maintained under hypoxia[5]. This selective regulation of translation under hypoxia is thought to largely be governed by features in 5'UTRs, including length, presence of secondary structures and/or specific motifs, including upstream open reading frames (uORFs)[20]. For example, some transcripts, such as ATF4, harbouring uORFs have enhanced translational efficiency under hypoxia[21].

Specific 5'UTR features have also been shown to render translation mTOR-sensitive. These features include the complexity and length of 5'UTRs[22] and the presence of 5'terminal oligopyrimidine (TOP) motifs[23,22,24]. Of note, TOP mRNAs largely encode proteins that are components of the translational machinery[25]. We previously observed an independent mechanism of selective translation of mRNAs encoding stem cell-associated factors (NODAL, SNAIL, NANOG), which is enabled by the presence of multiple 5'UTR isoforms. NODAL, SNAIL and NANOG protein levels accumulated under hypoxia despite marked reductions in global protein synthesis due to the presence of multiple 5'UTR sequences, at least one of which could be efficiently translated[26]. These findings raised the possibility that in addition to reprogramming of the translational machinery, changes in the composition of 5'UTRs may also drive adaptive translational regulation.

Here, by simultaneously profiling transcriptomes, epigenomes, 5'UTRomes and translatomes under normoxia and hypoxia, we uncovered a hitherto unappreciated mechanism of gene regulation wherein global modifications in the epigenome facilitate hypoxia-induced alterations in mRNA translation. On a genome-wide scale, we show that perturbations of H3K4me3 lead to massive alterations in TSS selection, remodeling the 5'UTRome. This global 5'UTR remodeling leads to a gain and/or loss of translation regulatory elements which, in cooperation with hypoxia-induced alterations of the protein synthesis machinery, enables the emergence of an adaptive translational response. For example, this mechanism of TSS switching is involved in regulating the synthesis of key factors, including pyruvate dehydrogenase kinase 1 (PDK1), implicated in metabolic adaptations to hypoxia. A large proportion of 5'UTR isoform changes occur for transcripts with unaltered overall transcript abundance and appear to be due to oxygen-dependent reductions in KDM5 activity, concomitant with an expansion of H3K4me3. Indeed, pharmacological inhibition of KDM5 can mimic hypoxia-induced switching events in the absence of HIF1 stabilization or significant alterations in mRNA abundance. Collectively, this work suggests that hypoxia-induced accumulation of H3K4me3 alters TSS selection, and that this previously unrecognized mechanism facilitates an adaptive translational response.

RESULTS

Hypoxia-induced TSS switching results in extensive remodeling of 5'UTRs.

We previously observed that several stem cell-associated factors have multiple 5'UTR isoforms, some of which are preferentially translated under hypoxia[26]. To determine whether this phenomenon occurs on a genome-wide level, we conducted nanoCAGE sequencing on total mRNAs extracted from T47D breast cancer cells as well as H9

human embryonic stem cells (hESCs) grown for 48 or 24 hours, respectively, in hypoxia (1% O_2) or normoxia (20% O_2) (**Fig 1A**). After preprocessing and alignment, this technique allowed for detection of approximately 20,000 RefSeq transcripts at a sequencing depth approaching saturation (**Fig S1A-B**). A transcriptional response was confirmed in both cell lines using principle component analyses and increased expression of hypoxia-associated transcripts (**Fig S1C; Fig 1B**). Consistent with our previous studies[22], we found that the length of expressed 5'UTRs often differed substantially from the annotations in the RefSeq database. When considering the weighted mean 5'UTR length (including all 5'UTR isoforms for a given transcript), the observed length was often substantially shorter than the annotated length (**Fig 1C**). Using all reproducible 5'UTR reads (those starting at exactly the same position across replicates), we defined clusters of TSSs for each transcript (described in detail in the methods) representing distinct 5'UTR isoforms. In total, we detected 77,487 and 72,993 TSS clusters in T47D and H9 cells, respectively, and found that 88% and 84% of protein-coding transcripts manifest more than one 5'UTR isoform, with the mean isoforms per transcript being between 3 and 4 (**Fig 1D-E**).

Next, we sought to determine whether 5'UTR availability may be regulated via TSS switching. Accordingly, we compared the pool of 5'UTR isoforms expressed in each condition. To focus on alterations affecting translation initiation without impacting on potential changes in translation caused by alterations in ORFs and/or events that could cause gain- or loss-of-function of the alternative proteoforms, we excluded TSS switching that would affect proteoform. Even with this exclusion, 21.5% of detected protein-coding transcripts underwent hypoxia-induced TSS switching that would alter 5'UTR sequence availability. To ensure that the phenomenon could extend across highly variant epigenomes, we conducted the same analysis in H9 cells and discovered that 28.3% of protein-coding transcripts had 5'UTR-altering TSS switching events (**Fig 1F-G**). Among the significant TSS switching events, we identified "quantitative changes" wherein the relative abundance of 5'UTR isoforms was altered (**Fig 1H**), as well as "qualitative changes" wherein condition-specific 5'UTR isoforms were gained or lost (**Fig. 1I**). Moreover, the analysis approach identifies TSS switches occurring in the presence (**Fig 1H**) or absence of changes in total transcript abundance (**Fig 1I**). Quantitative changes can be exemplified by SH3BP2, whereby overall transcript levels were significantly increased under hypoxia, occurring together with a switch from expression of shorter 5'UTR isoforms towards expression of longer isoforms (**Fig 1H**). In contrast, for PELP1, there was no change in overall transcript abundance, but a qualitative change whereby the TSS cluster producing the longest 5'UTR isoform was lost under hypoxia (**Fig 1I**). Interestingly, the large majority of TSS switching events occurred for transcripts where there were no significant changes in overall transcript abundance between hypoxia and normoxia-treated cells (79.7% and 77.3% for T47D

and H9, respectively), suggesting that altered transcription is not required for TSS switching to occur (**Fig 1J**). Together, these findings uncover widespread hypoxia-induced remodeling of 5'UTRs occurring largely in the absence of changes in overall mRNA abundance.

5'UTR and translational machinery remodeling are coordinated under hypoxia.

Translation is thought to largely be regulated by the interactions between 5'UTR features and protein synthesis machinery at the rate-limiting initiation step[20,27]. Therefore, we next sought to evaluate interactions between the 5'UTRome and remodeling of translation in hypoxia. To do this, we first performed transcriptome-wide profiling of mRNA translation using polysome-profiling followed by RNA sequencing[28]. In accordance with previous studies[3], hypoxia caused a 90% reduction in polysome/monosome ratios in both T47D and H9 cells (**Fig 2A, Fig S2A**), which are directly proportional to the levels of global protein synthesis[29] assuming rates of elongation are not impacted. This was concomitant with increased HIF1□ levels (**Fig 2B, Fig S2B**). Moreover, hypoxia suppressed mTOR signaling and induced ISR as illustrated by reduced phosphorylation of downstream substrates of mTORC1 (i.e., 4E-BP1 and rpS6) and increased phosphorylation of eIF2□, respectively (**Fig 2B, Fig S2B**). These changes were accompanied by reduced cyclin D3 protein levels (**Fig 2B**), which is encoded by an mRNA whose translation critically depends on the activity of the mTORC1/eIF4F axis[30].

To identify changes in translation efficiency, we compared total mRNA transcript levels to those isolated from heavy polysomes (>3 ribosomes) using the Anota2seq algorithm[31] (**Fig 2C, Fig S2C**). Notwithstanding that for a number of genes, changes in total mRNA abundance were congruent with alterations in loading to heavy polysomes, there were significant discordant alterations in levels of mRNA associated with heavy polysomes relative to total mRNA for more than 2,000 transcripts in each of the T47D and H9 cell lines (**Fig 2C, Fig S2C**), indicating that the translatome is extensively remodelled in hypoxia. Observed changes in translation could be grouped into two distinct regulatory modes: firstly, changes in polysome-association not accompanied by congruent changes in total mRNA levels (that will be referred to as "translation"), and secondly, changes in total mRNA levels that are translationally offset such that the polysome association is unaltered (that will be referred to as "offsetting"). Importantly, the "translation" mode of regulation results in altered protein levels, while "offsetting" opposes alterations in protein downstream of changes in mRNA abundance[32]. Consistent with previous findings[26], in T47D cells, hypoxia induced increases in mRNA abundance for genes related to cellular plasticity and EMT (cell migration, response to wounding) and decreases for genes related to DNA replication and oxidative

phosphorylation (**Fig S2D**). Translationally suppressed genes were enriched for processes involved in nucleosome organization, cytoplasmic translation, and oxidative phosphorylation, while those involved in DNA-binding transcription factor activity and EMT-related processes were translationally activated. Genes related to cell cycle, protein localization, and RNA processing were translationally offset (mRNA down) (**Fig S2D**). Furthermore, many processes were affected similarly in H9 cells (**Fig S2E**). Notably, genes related to cytoplasmic translation were strongly translationally offset (mRNA up) in both T47D and H9 cells and largely comprised of mRNAs with TOP motifs whose translation is highly mTOR-dependent[23,22,24] (**Fig S2F-G**). This suggests that the increase in TOP mRNA levels is translationally offset in hypoxia to prevent excessive production of the components of the translational machinery.

Having mapped the changes to the translatome that occur under hypoxia, we next sought to establish the links between regulatory pathways that impinge on the translational machinery and 5'UTR features contributing to translational regulation. To achieve this, we developed a method based on step-wise regression models that integrate pathways and mRNA features of 5'UTRs to identify variables that independently explain variance in the per-gene translation efficiencies measured in our translatome analysis (described in detail in STAR methods). Specifically, we were interested in the combinatorial effects of different pathways and mRNA features on the translation efficiency of an mRNA and how these variables may relate to each other. A series of signatures was created, where each signature included genes with translational regulation previously identified as downstream of pathways[33,21,34,35,36,37,38,39,40,41,42], as well as features of 5'UTRs characterized using the most abundant isoform detected under hypoxia in our nanoCAGE sequencing data. These included features like the 5'UTR length, GC content, the presence of uORFs and various known motifs like TOPs, as well as *de novo* motifs identified as enriched in subsets of transcripts regulated by translation or offsetting. In total, for T47D cells, the model identified variables that together explained 42.6% of the changes in translation (**Fig 2D**) and 31.7% of the changes in offsetting (**Fig 2E**) that occur in response to hypoxia.

Using this analysis, we confirmed that suppression of mTOR signaling and activation of the integrated stress response (ISR) play a large role in the reprogramming of the translatome under hypoxia, together accounting for 32.24% of translation changes and 10.72% of translational offsetting. Signatures of mTOR and ISR-sensitive translation were significantly anti-correlated with each other for the translation mode of regulation, demonstrating that the subsets of genes regulated by these pathways are largely distinct. We also found that 5'UTR GC content could independently explain 2.29% of translation changes and 4.15% of changes in offsetting, with higher GC being

associated with decreased translation efficiency upon hypoxia (**Fig 2F-G**). Furthermore, GC content was correlated with signatures of mTOR-sensitive translation, exposing a link between mTOR signaling and translation of transcripts with GC-rich 5'UTRs. Consistent with 5'UTR length and the presence of uORFs mediating selective translation downstream of mTOR-signaling and the ISR, respectively, these RNA features did not explain variance in translation or offsetting independently of these pathways. Moreover, both were significantly negatively correlated with mTOR-activated translation (r = -0.23, r = -0.14, respectively), suggesting that translation of mRNAs with longer 5'UTRs and uORFs are suppressed upon mTOR activation. Indeed, transcripts with short 5'UTRs were previously identified as translationally activated upon mTOR activation[22] while those harbouring uORFs were translationally suppressed[38]. Accordingly, the approach accurately recapitulates known relationships between key signaling pathways and RNA features mediating selective regulation of mRNA translation. Consistent with the observed gene ontology enrichments (**Fig S2D, S2E**), the TOPscore (a metric proposed by Philippe *et al.*[24] quantifying the presence and length of TOP motifs across all 5'UTR isoforms for a given transcript) was the strongest predictor of offsetting. Consistent with the mTOR-sensitivity of mRNAs with TOP motifs, TOPscore-associated offsetting overlapped with the signature of mTOR-activated translation (**Fig 2E**). In addition to mTOR and ISR-controlled translation, U34 tRNA modifications and RNA helicase DHX9-dependent signatures of translational regulation contributed to changes in translation independently of ISR and mTOR-sensitive translation, suggesting a previously unappreciated role in translational reprogramming for these factors in hypoxia. Furthermore, translation dependent on high expression of eIF4E could also explain proportions of variance in both translation and offsetting regulatory modes in a manner independent of mTOR signaling. Finally, we identified several sequence motifs in 5'UTRs associated with changes in translation and offsetting under hypoxia that were not significantly correlated with regulatory pathways reported to modulate protein synthesis machinery (**Fig 2D-G**). This suggests the existence of yet unknown regulatory mechanisms that are involved in shaping translatomes under hypoxia.

To examine how universal the roles of the variables that could independently explain changes in translation efficiency are in governing translational reprogramming under hypoxia, we repeated the analysis in the highly divergent H9 cell model. Here, using the same pathway and 5'UTR mRNA feature signatures, we explained 46.7% and 41.7% of the variance in translation and offsetting, respectively (**Fig S3A-B**). Similar to the T47Ds, we found that the suppression of mTOR and activation of the ISR accounted for the greatest proportion of changes in translation efficiencies, demonstrating that translational reprogramming under hypoxia is regulated by largely similar variables across highly diverse cell models. In addition, signatures associated with altered

translation downstream of phosphorylated eIF4E, eIF4G, and DAP5, as well as a set of, largely distinct from those identified in T47Ds, 5'UTR motifs also associated with altered translation (**Fig S3C-D**). Collectively, these findings highlight the high degree of coordination between regulatory pathways and 5'UTR features that govern adaptive changes in translation under hypoxia.

TSS switching contributes to translational reprogramming under hypoxia.

Having identified 5'UTR features and their crosstalk with signaling pathways in regulating translation initiation, we next sought to evaluate the impact of 5'UTR remodeling caused by TSS switching on translational adaptation to hypoxia. As changes in TSS usage between hypoxia and normoxia-treated cells were often complex and could affect multiple isoforms to different degrees (**Fig 3A**), we employed a method based on changepoint algorithms[43] to identify segments of 5'UTR sequences that were enriched or depleted under hypoxia as a result of TSS switching (see STAR methods). Using this approach, we identified the degree of enrichment of specific 5'UTR sequences and assigned a score describing the extent of isoform switching based on the maximum difference between enriched and depleted sequence windows (termed the TSS switch score). In the example provided for SLC25A20 (**Fig 3A**), changepoints where isoform expression diverged between conditions were identified at 58 and 91 nt upstream of the start codon (**Fig 3B**). The abundance of isoforms between these points was relatively enriched by more than 20% in hypoxia, with the concomitant depletion of 5'UTR isoforms longer than 91 nt (**Fig 3C**). A TSS switch score of 49.16 indicated a high degree of 5'UTR remodeling despite no significant change in overall transcript expression (**Fig 3D**). We next applied this method to all transcripts identified as having significant quantitative and qualitative changes in TSS usage between hypoxia and normoxia in T47D and H9 cells. Comparing the distributions of TSS switch scores between cell lines, it was observed that the T47D scores were somewhat right-shifted, indicating that although a greater number of significant switching events were identified in the H9 cells, the magnitude of the resulting differences in isoform expression tended to be greater in the T47Ds (**Fig 3E**). Furthermore, when comparing which 5'UTR sequence regions relative to the start codon were most commonly enriched under hypoxia, we found that in T47Ds there was an enrichment of either the shortest or the longest isoforms. This was in contrast to H9 cells, where 5'UTRs were predominantly lengthened (**Fig 3F**). In addition, we also compared the GC content of the hypoxia-enriched and -depleted 5'UTR sequence segments and found that hypoxia-enriched sequences became significantly more GC-rich in the T47D cells with increasing TSS switch scores (**Fig 3G**). A similar pattern was also observed in the H9 cells. However, the difference in GC was greater at lower TSS switch scores (> 15) and not apparent for transcripts with the highest TSS switch scores (> 50) (**Fig 3H**), possibly reflecting that,

in general, the differences in isoform expression were more modest in H9 relative to T47D cells, as well as the distinct pattern of gains of shorter vs longer isoforms (**Fig 3E-F**). Together, these findings suggest that although the global patterns of hypoxia-induced TSS switching may differ between the T47D and H9 cells, transcription appears to be more likely to initiate at GC-rich regions for transcripts that undergo 5'UTR remodeling under hypoxia. Alternatively, the stability of already expressed GC-rich isoforms may be selectively increased.

Having identified the segments of 5'UTR sequences that were most highly enriched or depleted under hypoxia at the isoform level, we next wanted to assess if the impact of this 5'UTR remodeling on translation efficiencies under hypoxia could be detected at the gene level. To do this, we repeated the step-wise regression modeling, adding signatures denoting hypoxia-induced 5'UTR remodeling, including the TSS switch score, and changes in 5'UTR length (based on the difference in weighted mean length of all 5'UTR isoforms between conditions). Including these signatures for the T47D dataset, the total proportion of variance in translation explained increased to 45.3% and to 35.9% for offsetting (**Fig 3I-J**). Notably, both changes in 5'UTR length and the TSS switch score were significant in the final model, explaining 0.95% and 1.54% of translation changes and 1.03% and 0.81% of offsetting changes, respectively (**Fig 3I-J**). These alterations were of similar magnitude to changes explained by activation of the ISR independently of mTOR-sensitive translation. Notably, more extensive TSS switching (higher TSS switch scores) was associated with translational activation under hypoxia (**Fig 3K**), while for offsetting TSS switching may oppose changes in transcript abundance to maintain protein homeostasis (**Fig 3L**). Furthermore, lengthening of the 5'UTR was associated with suppressed translation, while genes that were translationally offset to oppose increases in total mRNA levels tended to undergo 5'UTR shortening (**Fig 3K-L**). Collectively, this suggests that hypoxia-induced 5'UTR remodeling is a coordinated adaptive process that predicts the ensuing type of translational regulation.

Although the magnitude of 5'UTR sequence segment enrichment or depletion under hypoxia was more modest in the H9 cells, making it less likely to be able to detect resultant changes in translation efficiencies at the gene level, we repeated our modeling. Here, we found that the total variance in translation explained increased to 49.5% when TSS switching signatures were included, and that changes in TOP motifs (quantified as the difference in TOPscore[24] between hypoxia and normoxia) explained 2.06% of the variance in translation (**Fig S4A**), indicating that gain or loss of TOPs due to TSS switching altered the translatome under hypoxia in H9 cells (**Fig S4B**). Collectively, our analyses suggest that hypoxia-associated alterations in translational efficiency are driven by a collaboration between 5'UTR features that can be altered as a result of TSS switching and modifications to the translational machinery. Remarkably,

TSS switching is a previously unappreciated mechanism facilitating coordination between mRNA sequence features and the initiation of mRNA translation.

TSS switching orchestrates adaptation to hypoxia by regulating mRNA isoform availability and translation.

Having identified TSS switching as a regulator of mRNA translation in hypoxia, we next wanted to understand whether certain biological processes may be preferentially regulated in this manner. We found that gene ontology terms related to metabolism were enriched among transcripts that underwent significant 5'UTR remodeling under hypoxia in both T47D and H9 cells (**Fig 4A**). One of the most significant TSS switching events in both cell lines was for Pyruvate Dehydrogenase Kinase 1 (PDK1) (**Fig 4B, Fig S5A**). To survive hypoxia, cells must be able to switch from oxidative phosphorylation to glycolysis. This is accomplished, at least in part, through induction of PDK1, which phosphorylates Pyruvate Dehydrogenase (PDH), thereby preventing entry of pyruvate into the citric acid cycle and conserving it for other metabolic processes required for adaptation to hypoxia, including its reduction to lactate to regenerate NAD+ for subsequent rounds of glycolysis[44]. PDK1 transcription is induced under hypoxia by HIF1□[45]. In addition, PDK1 is activated by ATP, NADH and CoA while being inactivated by ADP, NAD+, pyruvate and CoA-SH[45]. We confirmed hypoxia increased HIF1□ protein levels in both T47D and H9 cells, and that this is concomitant with increased PDK1 protein as well as enhanced PDH1 phosphorylation at S232 (**Fig 4C**, **Fig S5B**). However, the mechanisms that allow translation of PDK1 mRNA when protein synthesis is globally reduced have remained elusive. Our changepoint analysis of 5'UTR isoform expression in T47D cells indicated that PDK1 undergoes TSS switching in response to hypoxia. PDK1 shows a loss of longer (> 87 nt) 5'UTRs in favor of shorter ones (< 87 nt) with a TSS switch score of 47.9, which indicates extensive changes in relative isoform abundance (**Fig 4D**). We confirmed expression of short, hypoxia-inducible isoforms using 5'RACE (**Fig 4B**), as well as isoform-selective Real-Time RT-PCR (**Fig 4E**). In the H9 cells, which are characterized by a more glycolytic state[46,3], more PDK1 5'UTR isoforms were detected under normoxia than in T47D cells (**Fig S5A**). Nevertheless, change points and sequence segment enrichments were similar (**Fig S5C**, suggesting that hypoxia-induced TSS switching may be an important regulator of PDK1 expression.

We next determined whether translation of 5'UTR isoforms of PDK1 depends on oxygen availability. To this end, we first monitored the distribution of endogenous 5'UTR isoforms across a sucrose gradient under normoxia or hypoxia (**Fig 4F**; albeit quantification of shorter isoforms will also include longer isoforms as these overlap). This revealed that the shorter (57 and 36 nt) hypoxia-enriched isoforms were associated with heavier polysomes and therefore more efficiently translated in normoxia, while

notably their translation efficiency was also higher relative to the longer (134 nt) 5'UTR isoforms under hypoxia (**Fig 4F).** These findings were further confirmed using dual luciferase reporter assays in HEK 293T cells (**Fig 4G**). As expected[47], hypoxia reduced translation driven by ACTB 5'UTR, while the translation of the reporter comprising 5'UTR of Activating Transcription Factor 4 (ATF4) was sustained (**Fig 4G**). Finally, as compared to the reporters comprising 5'UTRs of longer PDK1 isoforms (134 nt), translation of the reporters harboring 5'UTR of shorter PDK1 isoforms (57 and 36 nt) was also higher under conditions of mTOR inhibition (INK128) and ISR activation (thapsigargin; TG) (**Fig 4H**). Hence, TSS switching in PDK1 led to an increase in shorter 5'UTR isoforms that are more efficiently translated, even in hypoxia. Together, these data suggest that hypoxia-induced TSS switching remodels the proteome by perturbing the levels of 5'UTR isoforms that determine translational efficiencies. To this end, PDK1 protein synthesis under hypoxia appears to be mediated by a TSS selection-driven increase in shorter 5'UTR isoforms whose translational efficiency is higher than those harbouring long 5'UTRs, and are therefore more likely to outcompete other mRNAs for access to the limited translational machinery under hypoxia.

Epigenomic alterations govern translation-regulating TSS selection.

Having demonstrated that hypoxia induces extensive remodeling of 5'UTRs and adaptive translational reprogramming, we next wanted to interrogate mechanisms driving TSS switching. A previous study found that HIF1□ can induce TSS switching in VHL-null RCC4 renal cell carcinoma cells, and that this is correlated with alterations in translation[48]. Although we also observed TSS switching for some transcriptional targets of HIF1□, such as PDK1, we found that the vast majority of TSS switching events in both T47D and H9 cells occurred in the absence of changes in overall transcript abundance (**Fig 1J**), suggesting that hypoxia-induced TSS switching may be largely governed by mechanisms that are not directly related to HIF1. Recent studies have shown that hypoxia can broadly regulate the epigenome, reprogramming chromatin via vast alterations to histone methylation due to the loss of activity of oxygen-dependent JMJC domain-containing enzymes like KDM5A[7,6]. Since H3K4me3 marks transcriptional start sites, and the activity of KDM5 is reduced in hypoxia, we next sought to determine the extent to which alterations in H3K4me3 may correlate with TSS switching. As hypoxia leads to global accumulation of H3K4me3, we chose to examine differences in the distribution of the mark around TSSs rather than changes solely in the magnitude of the peaks. To do this, we generated three biological replicates of H3K4me3-ChIPseq from hypoxia and normoxia-treated T47D and H9 cells (**Fig S6A**), which revealed significant differences in H3K4me3 distributions around TSSs for almost all protein-coding genes detected by nanoCAGE sequencing (94.03% and 97.84% at FDR < 0.01 in T47D and H9, respectively) (**Fig 5A**). These changes in distribution fell into two

categories: The first category captured changes occurring in the absence of a clear directionality, exemplified by RIPK2 that undergoes TSS switching in T47Ds and where the mark appears to broaden around the TSS under hypoxia (**Fig 5B**). However, we also found that many of these changes in distribution had a significant directionality (45.24% in T47D and 89.91% in H9 cells) (**Fig 5C**), with the position of the peaks shifting up- or downstream under hypoxia, such as for PDK1 (**Fig 5D**). Significant TSS switching events were associated with both categories of H3K4me3 changes. However, as these alterations were almost universal, we narrowed our approach to focus on the effects of H3K4me3 alone.

If failure to remove H3K4me3 were mediating hypoxia-induced TSS switching, we would expect that inhibition of KDM5 may mimic certain TSS switching events observed under hypoxia. To test this, we treated T47D cells with the selective KDM5 inhibitor, C48 (10 mM; 24 h) (**Fig 5E, Fig S6B**), which led to a similar H3K4me3 accumulation as compared to 24 h of 0.5% O_2 (**Fig 5F**). Importantly, unlike hypoxia, C48 treatment did not induce HIF1□, or impact on mTOR or ISR signaling, as evidenced by the lack of changes in phosphorylation of S6 and eIF2□ with increasing C48 concentration (**Fig 5E, Fig S6B**). We next performed nanoCAGE sequencing to map TSSs in C48 and DMSO-treated T47D cells (**Fig S6C**) and found that C48 treatment was sufficient to induce TSS switching events for close to 1000 protein-coding transcripts (**Fig 5G**). Strikingly, this switching occurred almost completely in the absence of changes in overall transcript abundance, as C48 treatment resulted in differential expression of only 19 transcripts (FDR < 0.15) (**Fig S6D**), compared to the more than 2,500 significant changes in transcript abundance that occurred under hypoxia (**Fig S6E**). We then repeated the changepoint analysis and found that the TSS switch scores tended to be lower with C48 than with hypoxia treatment, suggesting that additional mechanisms, such as transcriptional changes, may tune the magnitude of the isoform switches under hypoxia (**Fig 5H**). To evaluate whether the TSS switching with C48 treatment could reproduce the TSS switching events observed under hypoxia, we compared the sequence segment enrichments between the two changepoint analyses. We determined that 27.13% (n = 477) of the transcripts that had significant TSS switching events under hypoxia (quantitative or qualitative changes) had the same sequence segment enrichments with C48 treatment. Using a Monte Carlo simulation-based approach, we determined that this was a greater proportion than could be expected to be the same by chance (20.6%). Furthermore, the proportion of equivalent TSS switching was significantly negatively correlated with the FDR of the TSS switching event under hypoxia, indicating that the more significant the TSS switching in hypoxia, the more likely to see the same pattern of changes with C48 treatment (**Fig 5I**). Of this subset of 477 transcripts that shared the same TSS switching patterns, close to 75% were not differentially expressed between hypoxia and normoxia (**Fig 5J**), further suggesting that

the changes in TSS usage were due to accumulation of H3K4me3, independent of additional factors like activation of hypoxic transcriptional programs.

To illustrate this, we examined procollagen lysyl hydroxylase 2 (PLOD2), which is known to be strongly induced under hypoxia by HIF1[49,50]. PLOD2 had a highly significant shift in H3K4me3 distribution around the TSS under hypoxia in T47D cells (**Fig 5K**). Moreover, PLOD2 underwent significant TSS switching under hypoxia, with a large enrichment in expression of 5'UTR isoforms longer than 194 nt. This pattern of TSS switching was precisely mirrored by C48 treatment, even in the absence of HIF1 induction or changes in overall transcript abundance (**Fig 5L-M**). We also examined the changepoints and sequence segment enrichments for PDK1 after C48 treatment, and despite the absence of transcriptional changes (that would increase the amplitude of the differences), we could still identify one of the same changepoints as in hypoxia, at 87 nt (**Fig S6F**), suggesting that H3K4me3 may play a role in priming TSS selection in the absence of changes in transcriptional activity. Furthermore, we also noted a weak relationship between the TSS switch score and changes in overall transcript abundance under hypoxia in T47D cells (r^2 = 0.035) (**Fig S6G)**, suggesting that transcription may potentiate the observed differences in 5'UTR isoforms for a only small subset of transcripts. However, in H9 cells there was little to no relationship (r^2 = 0.0002) (**Fig S6H**), consistent with that for the vast majority of transcripts the difference in abundance of 5'UTR isoforms and changes in overall transcript abundance are independent. Collectively, these data suggest that accumulation of H3K4me3, due to reduced KDM5 activity, is a major determinant of TSS selection under hypoxia, leading to extensive remodeling of 5'UTRs.

DISCUSSION

Understanding the mechanisms driving the acquisition of cellular plasticity in cancer remains critical to improving patient outcomes. Here, we have examined how a microenvironmental stress like hypoxia can rewire gene expression through the coordination of epigenetic, transcriptional, and translational programs. We have uncovered widespread changes in TSS usage occurring under hypoxia that lead to altered availability of 5'UTR sequences. This altered pool of 5'UTRs works in concert with reprogramming of the translational apparatus to mediate a survival-enhancing adaptive translational program. As part of this program, we observed that the switch towards glycolytic metabolism under hypoxia may be facilitated by a shift in expression towards shorter, more efficiently translated 5'UTR isoforms of PDK1. We also found that hypoxia-induced TSS switching was largely independent of changes in overall mRNA abundance, but instead could be reproduced solely through accumulation of H3K4me3 around TSSs as a result of reduced KDM5 activity in the absence of

activation of HIF1, or alterations in the translation initiation machinery. Together, these findings support an emerging paradigm of gene expression control whereby regulation of mRNA translation is directed at the level of chromatin modifications and is driven by alternate TSS selection giving rise to 5'UTR isoforms that are "tailored" to exhibit inherently higher translation efficiency. These isoforms thereby outcompete other mRNAs for access to the limiting protein synthesis machinery. Over 50 years ago, based on studies on hemoglobin synthesis, it was proposed that mRNA translation may be selectively modulated by altering the availability of the components of the translation initiation machinery[51]. This can largely be explained by the 5'UTR features that distinguish translationally "strong" mRNAs, that are efficiently recruited by the translation initiation apparatus, and can thus outcompete "weak" mRNAs for access to the protein synthesis machinery. In this context, our results suggest that H3K4me3-dependent TSS selection under hypoxia may be adjusting the abundance of "strong" vs. "weak" 5'UTR isoforms to remodel the proteome in response to hypoxia.

The majority of genes harbour multiple TSSs, with differential use being linked to tissue-specificity and disease states[52,53,54]. Altered TSS usage impacting the translatome has been reported between mammary epithelial cells MCF10A and MCF7 breast cancer cells[55], and our previous work identified a number of stem cell factors that manifest multiple 5'UTR isoforms with different translation efficiencies under hypoxia that arise from distinct TSSs[26]. Although TSS switching has a high potential to impact translation due to the inclusion or exclusion of 5'UTR regulatory elements, most studies to date have focused on usage of alternative promoters while examinations of TSS changes within the same promoter region have been lacking. Transcriptome-wide profiling of TSSs under hypoxia and normoxia in colon cancer cells identified 191 genes with differential promoter usage[56]. Here, we purposely focused on TSS switching events that would not alter the resulting proteoform, and profiled differences between isoforms within one promoter in order to capture changes that could impact on translation initiation. At this higher resolution, we revealed that TSS switching events under hypoxia are dramatically more widespread than previously appreciated, affecting more than 20% of protein-coding transcripts across highly divergent cell lines. The importance of this higher-resolution approach is illustrated by 5'UTR regulatory elements that are highly positional, such as TOP motifs, where a difference of only a few nucleotides could drastically alter translation of corresponding mRNAs[24]. Indeed, we found that TSS switching leading to changes in TOP motifs plays a significant role in translational reprogramming of H9 cells in response to hypoxia. Furthermore, changes in 5'UTR length that were often modest were unexpectedly found to be significantly associated with altered translation and translational offsetting under hypoxia, demonstrating the surprising impact of this relatively unappreciated regulatory mechanism.

The role of mTOR suppression and activation of the ISR in mediating global suppression of protein synthesis under hypoxia have been well established[5]. However, other mechanisms of translational reprogramming, in particular how selective translation of survival-promoting transcripts is enhanced or maintained, is less understood. Our study reveals a model whereby changes in 5'UTR composition are a driving force of adaptive translatomes via gain and/or loss of regulatory features, which is orchestrated with reduced availability of the protein synthesis machinery under hypoxia driven by the induction of ISR and inhibition of mTOR signaling. Moreover, our study identifies potential implication of other factors that are orchestrated by epigenetic remodeling of the 5'UTRome. These include U34 tRNA modifications[57], the RNA helicase DHX9[40], DAP5 that is involved in alternative cap-dependent initiation of translation in cancer cells[34], and alterations in eIF4E phosphorylation[58]. Interestingly, we also identified a number of previously unrecognized sequence motifs in 5'UTRs that were associated with translational activation under hypoxia, warranting future studies.

The precise role of H3K4me3 in mediating gene expression has been the subject of some debate[12,8]. It has been shown to participate in anchoring transcriptional machinery to nucleosomes, suggesting a role in transcriptional activation[59]. Furthermore, local induction of H3K4me3 was sufficient to enable transcription at silenced loci in several cell models[60]. In contrast to this, several studies have also demonstrated that loss of H3K4me3 has limited effect on transcription, and that this mark is not required for transcription to occur in most cases[8,12,61]. Here, we show that treatment with the KDM5 inhibitor C48, leading to accumulation of K3K4me3, resulted in only minimal changes in transcript abundance, supporting the tenet that increasing the mark alone is not sufficient to stimulate transcription. However, we observed that changes in TSS usage upon C48 treatment largely overlap with those that occur under hypoxia, suggesting that H3K4me3 plays an important role in precise TSS selection under different cellular conditions. A recent study in RCC4 renal cell carcinoma cells identified HIF-dependent changes in TSS usage, impacting on translation[48]. We also report significant TSS switching at HIF1 targets, including PDK1 and PLOD2. However, close to 75% of the TSS switching events we observed occurred for transcripts that exhibited no significant change in expression under hypoxia, indicating that TSS switching is mediated by events additional to HIF1-activated transcriptional programs, and occurs in the absence of modulation of mTOR signaling and the ISR.

In conclusion, we present a mechanism whereby translational adaptations under hypoxia are tuned by alterations in the availability of 5'UTR sequences that are coordinated by epigenetically-mediated changes at TSSs. These findings put forward a largely unappreciated paradigm that cellular stress can be sensed at the level of

chromatin to direct adaptive remodeling of the translatome thereby orchestrating plasticity-promoting gene expression programs.

Limitations of the study

In this study, we focused on the orchestration of the epigenetic events with the translation initiation under hypoxia. Hypoxia is, however, likely to also impact on the elongation phase of translation via, e.g., modulation of eEF2K activity[62] and/or changes in methylation of eEF1A[63]. Further studies are thus warranted to investigate whether hypoxia-driven epigenetic changes may lead to selective perturbations in elongation. In addition, although the total proportion of variance in translational changes explained by the signatures denoting changes to 5'UTRs as a result of TSS switching appeared quite modest in our models, this is likely to be an under-estimate of the impact of this mechanism on the translatome. This is because our translation efficiencies were calculated at the gene level rather than the isoform level, so it is likely that only the more extreme isoform-driven changes in translation efficiency would be captured. Furthermore, the models only considered genes that had significant changes in their translation or translational offsetting. However, for cases where there appears to be no change in regulation at the gene level, there may still be extensive changes in expression and translation of 5'UTR isoforms that serve to maintain constant protein levels. In the future, it will be of great interest to apply the methods developed in this study to more fully understand the mRNA features contributing to differential isoform-level translation.

STAR METHODS

Key resources table

REAGENT or RESOURCE	SOURCE	IDENTIFIER
Antibodies		
4E-BP1, phospho-S65	Cell signaling	Cat# 9451S
4E-BP1, phospho-T37/46	Cell signaling	Cat# 2855
4E-BP1 (35H11)	Cell signaling	Cat# 9644
S6 ribosomal protein, phospho-S240/244	Cell signaling	Cat#2215
S6 ribosomal protein (5G10)	Cell signaling	Cat# 2217
EIF2S1 [E90] phospho-S51	Abcam	Cat# ab32157
eIF2□	Cell signaling	Cat# 9722
HIF1□ (D1S7W) XP	Cell signaling	Cat# 36169
PDK1 [4A11]	Abcam	Cat# ab110025

PDHE1□ (D6)	Santa Cruz	Cat# sc-277092
PDHE1□ phospho-S232	EMD milipore	Cat# AP1063-50 µg
PDHE1□ phospho-S293 [EPR12200]	Abcam	Cat# ab177461
Cyclin D3 (DCS22)	Cell signaling	Cat# 2936
Histone H3 (D1H2) XP	Cell signaling	Cat# 4499S
Histone H3K4me3 (C42D8)	Cell signaling	Cat# 9751S
H3K4me3 antibody ChIP	Epigentek	A4033
□-tubulin (mouse)	LICOR	Cat# 926-42213
Beta-tubulin (rabbit)	LICOR	Cat# 926-42211
Beta-actin (mouse)	LICOR	Cat# 926-42212
Beta-actin (rabbit)	LICOR	Cat# 926-42210
IRDye 800CW anti-mouse	LICOR	Cat# 926-32212
IRDye 680RD anti-mouse	LICOR	Cat# 926-68072
IRDye 800CW anti-rabbit	LICOR	Cat# 926-32213
IRDye 680RD anti-rabbit	LICOR	Cat# 926-68073
Bacterial and virus strains		
One Shot™ MAX Efficiency™ DH5α-T1R Competent Cells	Invitrogen	12297016
Biological samples		
Chemicals, peptides, and recombinant proteins		
INK128 (MLN0128), mTOR inhibitor	Cell signaling	Cat#30695
Thapsigargin	Cell signaling	Cat#12758S
Compound 48	Axon Medchem	Axon 2809/batch1
Trizol™ reagent	Invitrogen	15596018
Trizol™ LS reagent	Invitrogen	10296028
Phenol:Chloroform:Iso-amyl alcohol (125:24:1)	Sigma-Aldrich	P1944-100ML
Phenol:Chloroform:IAA (125:24:1), pH4.3	Invitrogen	AM9720
Pierce RIPA Lysis and Extraction Buffer	Thermo Scientific	PI89900
Halt™ Protease and Phosphatase Inhibitor Cocktail, EDTA-free (100X)	Thermo Scientific	78445
3'-O-Me-m7G(5')ppp(5')G RNA Cap Structure Analog	NEB	S1411S
Ribonucleotide Solution Set	NEB	N0450L
T3 RNA Polymerase	NEB	M0378S

DNase I	NEB	M0303L
RNase Inhibitor, human placenta	NEB	M0307L
MegaClear Transcription clean up kit	Invitrogen	AM1908
DMRIE-C transfection reagent	Invitrogen	10459-014
FastDigest BAMHI	Thermo Scientific	FD0055
FastDigest Pfl23II (BsiWI)	Thermo Scientific	FD0854
Fastdigest XbaI	Thermo Scientific	FD0684
Fastdigest MluI	Thermo Scientific	FD0564
Fastdigest NdeI	Thermo Scientific	FD0583
MNase	Worthington Biochemical Corp.	LS004797
Critical commercial assays		
Dual-luciferase reporter assay system	Promega	E1910
FirstChoice™ RLM-RACE Kit	Invitrogen	AM1700
Illustra GFX PCR DNA and gel band purification kit	GE healthcare	Cat# 28903470
SuperScript™ IV VILO™ Master Mix with ezDNase™	Invitrogen	11766050
SYBR™ Green PCR Master Mix	Applied Biosystems	4364346
AmpliTaq Gold™ 360 Master Mix	Applied Biosystems	4398881
NEBuilder HiFi DNA Assembly Cloning Kit	NEB	E5520S
TOPO™TA Cloning™ kit for sequencing (pCR 4-TOPO)	Invitrogen	450030
QIAquick PCR Purification Kit	Qiagen	28104
MinElute PCR Purification Kit	Qiagen	28004
Micro BCA™ Protein Assay Kit	Thermo Scientific	23235
Mycoplasma detection kit ATCC	ATCC	30-1012K
Deposited data		
Raw and processed data	This paper	GEO: Pending publication
eIF4G-dependent translation signature	Ramírez-Valle et al.[35]	GSE11011
DAP5-dependent translation signature	de la Parra et al.[34]	GSE115142
mTOR-dependent translation signature	Gandin et al.[38]	GSE76766
Experimental models: Cell lines		

T47D ductal carcinoma cells	ATCC	HTB-133
HEK 293T cells	ATCC	CRL-3216
H9 human embryonic stem cells (hESCs)	WiCell, Madison, WI, USA	WA09
Experimental models: Organisms/strains		
Oligonucleotides		
Ultramer oligo 36nt-PDK1: gctatgaccatgattacgccaagcgcgcACGCGTAATTAACCCTCACTAAAGGGGCGTACTGGCTGTGGCTTCTCTAGCGGGACTCGGCCAtatgGAAGACGCCAAAAACATAAAGAAAGG	IDT	
qPCR primers see supplemental file S1	Thermofisher	
Cloning primers see supplemental file S1	Thermofisher	
RACE primers see supplemental file S1	Thermofisher, Invitrogen	
nanoCAGE primers see supplemental file S1	Thermofisher, Illumina	
Recombinant DNA		
pKS-FF-HCV-Ren	gift from J. Pelletier	Steinberger et al.[64]
gBlocks see supplemental file S1	this paper	N/A
pKS-beta-actin-FF-HCV-Ren	this paper	N/A
pKS-ATF4-FF-HCV-Ren		
pKS-134nt-PDK1-FF-HCV-Ren	this paper	N/A
pKS-57nt-PDK1-FF-HCV-Ren	this paper	N/A
pKS-36nt-PDK1-FF-HCV-Ren	this paper	N/A
pUltra-SV40-134nt-PDK1-EGFP	This paper	N/A
pUltra-SV40-57nt-PDK1-EGFP	This paper	N/A
pUltra-SV40-36nt-PDK1-EGFP	This paper	N/A
pGL4.13_BsiWI-PacI	Gift from Ola Larsson	
pDONR223-PDK1	Gift from William Hahn, David Root[65]	Addgene plasmid #23804
Software and algorithms		

ImageStudio Acquisition Software	LICOR	https://www.licor.com/bio/image-studio/
nf-core/chipseq pipeline v.1.2.0	Nf-core	https://github.com/nf-core/chipseq
Bowtie (version 1.2.2)	Langmead et al.[66]	https://bowtie-bio.sourceforge.net/index.shtml
Bedtools (v2.29.1)	Quinlan et al.[67]	https://bedtools.readthedocs.io/en/latest/index.html
BBTools	Bushnell B.	http://sourceforge.net/projects/bbmap/
HISAT2	Kim et al.[68]	http://daehwankimlab.github.io/hisat2/
RSubreads	Liao et al.[69]	https://bioconductor.org/packages/release/bioc/html/Rsubread.html
Anota2seq	Oertlin et al.[31]	https://bioconductor.org/packages/release/bioc/html/Anota2seq.html
Cytoscape (v.3.8.2.)	Shannon et al.[70]	https://cytoscape.org/
ClueGO (v.2.5.8)	Bindea et al.[71]	https://apps.cytoscape.org/apps/cluego
TagDust (version 2.33)	Lassmann[72]	https://github.com/TimoLassmann/tagdust
Cutadapt (version 1.18)	Martin[73]	https://cutadapt.readthedocs.io/en/stable/

Perl script for removal of strand invasion artifacts	Tang et al.[74]	Script provided in supplemental data of Tang et al.[74]
limma	Ritchie et al.[75]	https://www.bioconductor.org/packages/release/bioc/html/limma.html
DESeq2	Love et al.[76]	https://www.bioconductor.org/packages/release/bioc/html/DESeq2.html
R	R Core Team	https://www.r-project.org/
ggplot2	Wickham[77]	https://ggplot2.tidyverse.org/
changepoint	Killick et al.[43]	https://cran.r-project.org/web/packages/changepoint/
Original code	This paper	Github repository: Pending publication
Other		
OxyCycler model C42	Biospherix	
ProOx model C21	Biospherix	
GloMaxÒ Navigator Luminometer	Promega	GM2010
Spectramax ABS plus plate reader		
Nitrocellulose membrane, 0.45µm	BioRad	1620115
LI-COR Odyssey CLx imaging system		
Ultracentrifuge Optima XPN-80	Beckman Coulter	
Rotor SW41Ti	Beckman Coulter	
Biocomp Gradient Master 108	Biocomp	
Polypropylene tubes 14 x 89 mm	Beckman Coulter	331372

Density gradient fractionation system	Brandel	Cat# BR-188-177
Dynabeads™ Protein A	Thermo Scientific	Cat# 10001D
Dynabeads™ Protein G	Thermo Scientific	Cat# 10003D
Qubit dsDNA Quantitation, Broad Range	Thermo Scientific	Cat# Q32850
Qubit dsDNA Quantitation, High Sensitivity	Thermo Scientific	Cat# Q32851
HAP resin	Bio-Rad	Cat#157-0021
Ultrafree-MC Centrifugal Filter	Millipore	UFC30HV25
Corning® Matrigel® hESC-Qualified Matrix	Stemcell Technologies	#07181
mTeSR™1 feeder-free medium supplemented with mTeSR™1 5X Supplement	Stemcell Technologies	#85850
StemPro™ EZPassage™ Disposable Stem Cell Passaging Tool	Thermofisher	23181010
RPMI-1640 Medium	Gibco	#11875093
DMEM	Gibco	#10566-024

Primer sequences

All primer sequences provided in **Supplemental File S1.**

Resource availability

Lead contact

Lynne-Marie Postovit: l.postovit@queensu.ca

Materials availability

Further information and requests for resources and reagents should be directed to and will be fulfilled by the lead contact.

Experimental model and subject details

Cell lines

T47D cells (ATCC, Manassas, Virginia, USA) were grown in RPMI-1640 Medium (Gibco, Cat#11875093) with 10% fetal bovine serum (FBS) (Corning). 293T cells were grown in DMEM (Gibco, Cat#10566-024) with 10% FBS. Cells were maintained using standard procedures. Cells were authenticated at the Sick Kids Research Institute and tested for mycoplasma (Mycoplasma detection kit, ATCC). H9 hESCs were obtained from WiCell, and the use of hESCs was approved by the Stem Cell Oversight

Committee of Canada. hESCs were cultured on plates prepared with Corning® Matrigel® hESC-Qualified Matrix (#07181, Stemcell Technologies) and fed daily using pre-warmed mTeSR™1 feeder-free medium supplemented with mTeSR™1 5X Supplement (#85850, Stemcell Technologies). Colony quality, confluence, and spontaneous differentiation were visually monitored daily, and differentiated colonies were manually scraped off the plate. hESCs were passaged using StemPro™ EZPassage™ Disposable Stem Cell Passaging Tool (23181010, Thermo Fisher). All tissue cultures were maintained at 37°C and 5% CO2 in a humidified environment.

Plasmids

The 5'UTR sequences of beta-actin (NM_001101.5) and mouseATF4 (NM_009716.3), and the sequences spanning 134 nt and 57 nt of the PDK1 5'UTR were synthesized as gBlocks (IDT) containing the T3 promoter and upstream *Nde*I and downstream *Mlu*I restriction sites. They were subcloned into the bicistronic luciferase reporter pKS-FF-HCV-Ren66 using a standard restriction digest/T4 DNA ligation protocol. The shorter 36 nt 5'UTR of PDK1 was synthesized as Ultramer DNA oligo containing the T3 promoter sequence and flanking sequences overlapping the digested vector. They were inserted into the digested pKS-FF-HCV-Ren plasmid using the NEBuilder HiFi DNA Assembly Cloning Kit.

The plasmid pGL4.13_134nt-PDK1 containing the 134 nt long 5'UTR and the complete ORF of PDK1 was constructed as follows. The 134 nt 5'UTR was amplified by PCR (primer pair PDK1-UTRstd_forw and PDK1_UTRstd_rev) from the pKS-134nt-PDK1-FF-HCV-Ren plasmid. The PDK1 open reading frame (ORF) was amplified from pDONR223-PDK1 (addgene #23804) (primer pair PDK1_ORFstd_forw and PDK1_ORFstd_rev). A pGL4.13 plasmid, modified by introduction of a *BsiW*I restriction site downstream of the SV40 promoter (pGL4.13_BsiWI-PacI), was digested with *BsiW*I (Pfl23II) and *Xba*I to excise the 5'UTR and luciferase ORF. The two PCR fragments containing the PDK1 5'UTR and the PDK1 ORF were inserted into the digested vector using the NEBuilder HiFi DNA Assembly Cloning Kit, creating the plasmid pGL4.13_134nt-PDK1. All cloning/propagation was performed in One Shot™ MAX Efficiency™ DH5α-T1R Competent Cells. All plasmids were confirmed by Sanger sequencing.

Method details

Cell culture experiments

For all experiments, T47D cells were plated 24 h prior to the treatment (1.2 x 10^6 in 60 mm dishes or 5.8 x10^5 in 6-well plates). For hypoxia experiments, media was changed

to fresh RPMI 10% FBS and cells were incubated in normoxia (regular incubator) or hypoxia (Biospherix OxyCycler model C42 or ProOx model C21 chambers housed in a regular incubator) at 0.5% O_2 for the indicated time. For hypoxia time course experiments, all cells received fresh media at the start time. 48 h hypoxia samples were placed in the hypoxia chamber at the start of the time course. 0h hypoxia samples were incubated in normoxia for 48 h. All other time points were incubated in normoxia until shifting them to hypoxia at 6, 12 or 24 h before the 48 h collection time point.

For mTOR inhibition, media was replaced with fresh RPMI 10% FBS containing 100 nM INK128. For compound 48 (C48) treatments, media was replaced with fresh RPMI 10% FBS containing 10µM C48 or the equivalent volume of DMSO as vehicle control. For the C48 dose-response experiments, media was replaced with a 1:10 dilution series starting at 10 µM C48 in RPMI 10% FBS.

RNA extraction and quantitative RT-PCR

T47D cells were placed on ice and washed with ice-cold PBS. 1 mL of Trizol was added, and cells were incubated at room temperature for 5 minutes. RNA was extracted as per manufacturer's instructions, and RNA pellets were resuspended in RNase and DNase-free H_2O. RNA concentration was determined with a Nanodrop and stored at -80˚C. Fractions from polysome gradients were extracted using 1 mL Trizol LS reagent according to the manufacturer's instructions. 500 ng RNA was reverse transcribed using the SuperScript™ IV VILO™ Master Mix with ezDNase™ at 55˚C extension temperature according to the manufacturer's instructions. After the RT reaction, cDNA was diluted 5-fold with H_2O and 1 µl per replicate was used in all following real-time quantitative PCR (qPCR) reactions.

qPCRs specific for the PDK1 5'UTR isoforms were performed using the SYBR™ Green PCR Master Mix. The primer pair PDK1_93/80nt amplifies all PDK1 transcripts with 5'UTRs longer than 78nt, primer pair PDK1_57/51nt amplifies all transcripts with 5'UTRs longer than 45 nt, and primer pair PDK1_ex2 amplifies all PDK1 transcripts. Relative amounts were determined using the relative standard curve method with a 1:4 serial dilution using cDNA from a hypoxia-treated sample.

To determine the relative contribution of the three main clusters of PDK1 5'UTR isoforms (longer than 78nt, between 78nt and 45nt and shorter than 45nt) to the total transcript level (**Fig. 4E**), the qPCR setup was modified as follows. qPCRs were performed as described above, except that the relative standard curve method was performed on a 1:5 dilution series of a linearized plasmid containing the full 134 nt of the 5'UTR plus the open reading frame (pGL4.13_134nt-PDK1) starting with 1 pg/µl of

plasmid. The result of the qPCR with primer pair PDK1_93/80nt represents the UTR isoforms longer than 78 nt. The result of the qPCR with primer pair PDK1_57/51nt represents the transcripts longer than 45 nt, i.e., also includes the transcripts longer than 78nt. The result of the qPCR with primer pair PDK1_ex2 represents all transcripts. The relative amount of just the mid-length or the short cluster was calculated as follows: mid-length = qPCR PDK1_57/51nt – qPCR PDK1_93/81nt: short = qPCR PDK1_ex2 – qPCR PDK1_57/51nt. The relative contribution to the total transcript level was calculated as the ratio of the relative amount of each cluster versus the relative amount of total transcript.
All qPCR reactions were run in triplicates on a QuantStudio5 or Viia7 cycler and analyzed using the QuantStudioTM Design & Analysis software v1.5.2 or the QuantStudio Real-time PCR software v1.6.1.

RLM-RACE

RNA ligase-mediated rapid amplification of cDNA ends (RLM-RACE) was performed with the FirstChoice™ RLM-RACE Kit (Invitrogen, AM1700) according to the manufacturer's instructions. In short, 10 µg of RNA isolated from normoxia and hypoxia-treated T47D cells was treated with calf intestinal phosphatase (CIP) to remove the 5'-phosphate from all molecules that contain free 5'-phosphates. RNA was extracted with acidic phenol/chloroform to remove CIP. The RNA was then treated with tobacco acid pyrophosphatase (TAP) to remove the cap structure from the full-length mRNA, leaving a 5'-monophosphate. A synthetic 5'RACE RNA adapter was ligated to molecules containing a 5'-phosphate. 2 µl of the ligated RNA was reverse transcribed using the SuperScript™ IV VILO™ Master Mix (Invitrogen) at an extension temperature of 55°C. 1 µl cDNA was used to perform nested PCR with forward primers specific for the 5'RACE adapter sequence (5'RACE_outer or 5'RACE_forw_inner) and reverse primers specific for PDK1 (PDK1_rev_outer, PDK1_rev_inner) and the AmpliTaq Gold™ 360 Master Mix. The first round PCR cycling conditions were 95 ºC for 10 min for polymerase activation, followed by 32 cycles of 95ºC for 30 sec denaturation, 59ºC for 30 sec annealing and 72 ºC for 1 min extension, followed by 72ºC for 7 min extension and 4ºC on hold. The second round PCR cycling conditions were 95 ºC for 10 min for polymerase activation followed by 35 cycles of 95ºC for 30 sec denaturation, 58ºC for 30 sec annealing and 72 ºC for 1 min extension, followed by 72ºC for 7 min extension and 4ºC on hold. PCR products were separated on a TAE/agarose gel, excised and extracted using a GE gel extraction kit. The purified PCR fragment was then inserted into the vector pCR4-TOPO using the TOPO™TA Cloning™ kit and One Shot™ MAX Efficiency™ DH5α-T1R Competent Cells. Plasmids were extracted using the Qiagen Plasmid mini kit, and the sequence of the 5'ends of the PDK1 transcripts was determined by Sanger sequencing.

Polysome profiles

T47D cells (8 x 10^6 cells per condition) were seeded in 15 cm plates 24 h prior to the experiment. Media was changed to fresh RPMI 10% FBS before cells were exposed to normoxia or hypoxia (0.5% O_2) for 24 h as described above. Polysome profiles were generated as previously described[78]. Cells were pre-treated with 100 µg/mL cycloheximide for 5 min and scraped in ice-cold, cycloheximide supplemented (100 µg/mL) PBS, using rubber scrapers. Cells were then pelleted in 15 mL conical tubes at 240 × g for 5 min at 4°C, and lysed on ice in 500 µL of hypotonic lysis buffer (5 mM Tris–HCl, pH 7.5, 2.5 mM $MgCl_2$, 1.5 mM KCl, 100 µg/mL cycloheximide, 1 mM DTT, 0.5% Triton, 0.5% sodium deoxycholate) for 15 min. Subsequently, lysates were cleared through a 15 min, 20 817 × g centrifugation at 4°C. Cleared lysates were diluted with hypotonic lysis buffer to set their optical density (OD) at 260 nm to 10–20. Sucrose gradients (5–50%) were generated in polypropylene tubes (Beckman Coulter, 331372, 14 × 89 mm) using a gradient maker (Biocomp Gradient Master 108), according to the manufacturer's instructions. A volume of 500 µL was removed from the top of the sucrose gradient to allow for sample loading. Lysates were then carefully layered over the top of linear sucrose gradients and centrifuged at 4°C for 2 h at 222 228 × g (36 000 rpm) using an ultracentrifuge (Beckman Coulter, Optima XPN-80, rotor SW41Ti), while 10% of the sample was kept as input. Ultracentrifuged samples were fractionated into 2 mL tubes using a density gradient fractionation system (Brandel, BR-188-177), resulting in 12 fractions of 800 µL each. Input samples, as well as sucrose gradient fractions, were mixed with 1000 µL of TRIzol LS reagent (Invitrogen) and kept at −80°C for subsequent RNA isolation.

Native ChIP-seq

Chromatin immunoprecipitation (ChIP) was used to analyze histone modifications. This protocol is based on previously published protocols from Shah et al.[79]. Three biological replicates were obtained for each cell line used. Post hypoxia treatment, control and treated cells were washed 2x in PBS and collected (500 rcf for 5 min at 4°C). Cell pellet volume was assessed before being flash frozen. Prior to each ChIP, antibodies were conjugated overnight at 4°C in ChIP Buffer 1 (25 mM Tris pH 7.5, 5 mM $MgCl_2$, 100 mM KCl, 10% glycerol, 0.1% NP-40, 200 uM PMSF, 50 µg/mL BSA) with 50/50 mix of Dynabeads™ Protein A (Thermo Fisher, 10001D) and Dynabeads™ Protein G (Thermo Fisher, 10003D) at a ratio of 6 µg of antibody to 25 µLof beads per sample. Prior to IP, beads were washed 2x with ChIP Buffer 1 and resuspended in 25 µL of ChIP Buffer 1. Frozen cells were washed twice in Buffer N (15 mM Tris Base, 15 mM NaCl, 60 mM KCl, 8.5% sucrose, 5 mM $MgCl_2$, 1 mM $CaCl_2$, 1 mM DTT, 200 uM PMSF, 1x protease

inhibitor, 50 µg/mL BSA), then resuspended in 2x cell pellet volume of Buffer N and lysed for 10 min on ice in equivalent volume of 2x Lysis Buffer (1x Buffer N, 0.6% NP-40). Nuclei were pelleted (500 rcf for 5 min at 4°C) and resuspended in 6x cell pellet volume of Buffer N, then spun through Sucrose Cushion (15 mM Tris Base, 15 mM NaCl, 60 mM KCl, 30% sucrose, 5 mM $MgCl_2$, 1 mM $CaCl_2$, 1 mM DTT, 200 uM PMSF, 1x protease inhibitor, 50 µg/mL BSA) at 500 rcf for 12 min at 4°C. Nuclei pellet was resuspended in 2x cell pellet volume of Buffer N. 2 µL of nuclei suspension was diluted with 18 µL of 2 M NaCl in triplicate, vortexed, and sonicated with a water bath sonicator (30x cycle of 30 seconds on, 30 seconds off) prior to measuring the chromatin concentration with NanoDrop Spectrophotometer (Thermo Fisher). The concentration of nuclei suspension was then adjusted to 1 µg/µL and separated into 100 µg chromatin aliquots. In the case of excess nuclei, unused aliquots were flash frozen.

Nuclei suspensions were prewarmed for 2 min at 37°C, then 1.5 µL of MNase (Worthington Biochemical Corporation, LS004797) was added for 12 min at 37 °C on a ThermoMixer (Eppendorf) set to 900 rpm. Digestion was stopped by adding 1/10 volume of MNase Stop Buffer (100 mM EDTA and 10 mM EGTA) and placing nuclei on ice. 5 M NaCl was slowly added to the suspension to a concentration of 0.6 M on the slowest vortex setting to release the chromatin, insoluble nuclei was then pelleted (18,000 rcf, 1 minute, 4 °C), and supernatant was run through hydroxyapatite (HAP) chromatography. 15 µL of soluble chromatin was saved for visualization and the rest of the soluble chromatin was added to 0.07 g of HAP resin (Bio-Rad, #157-0021) rehydrated in HAP Buffer 1 (5 mM NaPO4 pH 7.2, 600 mM NaCl, 1 mM EDTA, 200 uM PMSF) and rotated for 10 min at 4 °C. HAP mixture was run through Ultrafree-MC Centrifugal Filter (Millipore, UFC30HV25) at 600 rcf for 30 seconds at 4 °C and 15 µL of flow-through was saved for visualization. Then the column was washed 4x with 200µL HAP Buffer 1, 4x with 200 µL HAP Buffer 2 (5 mM $NaPO_4$ pH 7.2, 100 mM NaCl, 1 mM EDTA, 200 uM PMSF), and eluted 3x with 100 µL of HAP Elution Buffer (500 mM $NaPO_4$ pH 7.2, 100 mM NaCl, 1 mM EDTA, 200 uM PMSF). Flowthrough after each step was saved for visualization. Chromatin concentration was measured again in triplicate with the combined HAP elutions using NanoDrop. Final chromatin concentration was adjusted to 20 ng/µL using ChIP Buffer 1 prior to IP.

15 µL of chromatin was set aside for input control and chromatin was added to beads conjugated with H3K4me3 antibody (Epigentek, A4033). Chromatin and bead mixture was rotated for 10 min at 4 °C, washed 2x with ChIP Buffer 2 (25 mM Tris pH 7.5, 5 mM $MgCl_2$, 300 mM KCl, 10% glycerol, 0.1% NP-40, 200 uM PMSF, 50 µg/mL BSA), washed 1x ChIP Buffer 3 (10 mM Tris pH 7.5, 250 mM LiCl, 1 mM EDTA, 0.5% Sodium Deoxycholate, 0.5% NP-40, 200 uM PMSF, 50 µg/mL BSA), and washed 1x with TE buffer, transferring beads to a new tube after each wash step. DNA was finally eluted in

50 µL of ChIP Elution Buffer (50 mM Tris pH 7.5, 1 mM EDTA, 1% SDS) at 600 rpm for 10 min at 55 °C on a ThermoMixer. 35 µL of ChIP Elution Buffer was also added to the input control to bring the final volume to 50 uL. To both input and eluted ChIP DNA, 2 µL of 5 M NaCl, 1µL of 500 mM EDTA, and 1 µL of 20 mg/mL Proteinase K was added and incubated for 2 hours at 55 °C and DNA was purified using MinElute PCR Purification Kit (Qiagen, 28004). DNA as eluted in ultrapure H_2O and concentration was measured before and after purification using Qubit dsDNA Quantitation, High Sensitivity (Thermo Fisher, Q32851). Finally, HAP input and elutions were visualized using 2% agarose gel in 1x TBE ran at 140 V for 40 min to confirm fragment sizes.

ChIP DNA was sent to the McGill University and Genome Quebec Innovation Center, where it was further validated via Bioanalyzer, followed by shotgun library preparation, and library sequencing via Illumina NovaSeq6000. H3K4me3 ChIP DNA was sequenced to a depth of about 50 million reads and input samples were sequence to a depth of about 150 million reads.

Analysis of H3K4me3 ChIP-seq data

Raw H3K4me3 fastq files were processed using the nf-core/chipseq pipeline v.1.2.0 (available at https://github.com/nf-core/chipseq)[80]. Reads were aligned to GRCh38/hg38 in paired-end mode and all other parameters were kept as default. The output of the pipeline includes BAM files with aligned reads with duplicates, multi-mapping, unpaired, and ENCODE blacklist[81] reads filtered out. In order to assess shifts in the position of H3K4me3 marks relative to TSSs of protein-coding genes, the data was converted to a transcript- rather than genome-centric format to facilitate comparisons to TSSs mapped using nanoCAGE sequencing. To do this, the filtered aligned reads were extracted from the BAM files and re-aligned to a custom index of 5'UTR genomic sequences using Bowtie (version 1.2.2)[66] (settings: -v 2 -X 1000 -a). This custom index was created from genomic sequence regions corresponding to RefSeq transcripts[82], with 2,000 bp of sequence added upstream of the annotated TSS, and 10,000 bp added downstream of the TSS. Bedtools genomeCoverageBed (v2.29.1) was then used to compute the genome coverage of H3K4me3 with -dz and -pc options, and -scale to normalize for library size. The cumulative sum of H3K4me3 coverage was calculated for each genomic region corresponding to RefSeq transcripts, and genomic regions were trimmed at the position where 95% of the cumulative H3K4me3 signal had already occurred. This was found to be necessary as H3K4me3 signals had variable degrees of extension around TSSs, such that the selected 12,000 bp window was not appropriate for all genes. In order to reduce file sizes and computation time, the position (relative to the TSS), and the H3K4me3 coverage were collected for every 0.1% increase in the cumulative sum of H3K4me3 signal, such that each genomic region corresponding to

RefSeq transcripts would have 1,000 data points summarizing the distribution of the histone mark. Genomic regions corresponding to RefSeq transcripts were filtered out if they had a maximum scaled read coverage below 0.8, or if the background signal (from input control samples) was above 0.6.

To assess whether there were significant changes in the distribution of H3K4me3 around the TSSs for protein-coding genes, the data were filtered to only include transcript IDs that were detected in our nanoCAGE datasets for T47D and H9 cells. To detect directional shifts in the position of H3K4me3 signal around TSSs between hypoxia and normoxia, a two-sided Wilcoxon Mann-Whitney test was applied to the distributions of positions where 0.1% increases in the cumulative H3K4me3 signal had occurred for each condition. The directionality of the H3K4me3 shifts (upstream or downstream), were determined by the difference between the positions of the distributions at the 25th, 50th, and 75th quantiles. To identify cases where a change in the distribution of the H3K4me3 mark had occurred, but without a defined directionality (e.g., a broadening of the peak, that extends both upstream and downstream), a two-sided Kolmogorov-Smirnov test was applied. *P*-values were adjusted for multiple testing using the Benjamini-Hochberg method, with a significance threshold of FDR < 0.01. As the biological replicates in both cell lines were reproducible (**Fig S6A**), the mean of the position distributions across the 3 replicates was used in statistical tests. Empirical cumulative distribution function, and scaled coverage plots show the mean of the replicates, with the standard deviation from the three biological replicates shaded.

NanoCAGE library preparation, sequencing, and data preprocessing

The quantity and quality of total RNA from hypoxia-treated T47D and H9 cells were assessed by Qubit (Life Technologies) and Bioanalyzer (Agilent Technologies), and 75 ng of RNA was used as input material to prepare nanoCAGE libraries as described previously[57,22] (T47D n = 3, H9 n = 4). Note that the Template Switching Oligonucleotides (TSO) include 8 nt random unique molecular identifiers (UMIs) that allow for identification of duplicate transcripts arising from PCR amplification, and one of six barcodes for increased multiplexing (ACAGAT, GTATGA, ATCGTG, GAGTGA, TATAGC, GCTGCA). Sequencing was performed at the SciLifeLab NGI (Sweden) facility using the HiSeq2500 (HiSeq Control Software 2.2.58/RTA 1.18.64) with a 100-base pair single-end setup using HiSeq Rapid SBS Kit vs chemistry. Bcl to fastQ conversion was carried out using bcl2fastq_v2.19 from the CASAVA software suite. The quality scale was Sanger/phred33/Illumina 1.8+.

NanoCAGE sequencing reads with each of the six barcodes were extracted using TagDust (version 2.33)[72], and Nextera XT N-Series 3' adapters were trimmed using

Cutadapt (v1.18)[73] (settings: -e 0.15 -01 -n 4 -m 25). PCR duplicates were defined as reads with identical UMI and sequence in the first 25 bp, and were filtered to keep only one unique read. We have found this step to be essential for the quality of the downstream analysis. Ribosomal RNA was removed using bbduk.sh from the BBTools software suite, with default settings. A summary of the nanoCAGE preprocessing can be seen in **Fig S1A**. Next, reads were aligned to the human genome hg38 using Bowtie (v1.2.2)[66] (settings: -a -m 1 --best --strata -n 2 -l 28), and reads that uniquely aligned or failed to align were collected for a second alignment step to a custom index of 5'UTR sequences. This custom index was created by extending RefSeq 5'UTR sequences[82] by 78 bases upstream using genomic sequence, and 78 bases downstream using mRNA sequences. These extensions were selected based on the criteria that the nanoCAGE read architecture allows for a maximal length of 78 after adapter trimming. Alignment to the custom index was also performed using Bowtie (settings: -a --best –strata -n 3 -l 25). Reads were trimmed by 1-2 based at the 5' end in the event of alignment mismatches at the first or second positions, and strand invasion artefacts were removed using the perl script provided by Tang et al.[74] (settings: -e 2).

Analysis of differential TSS usage

Transcription start site peaks were defined as the 5' end mapping positions of reads for each sample. Peaks that were observed in less than n -1 samples per condition were excluded to select only those that were reproducible. RefSeq transcripts with fewer than 10 reads were excluded before assessing library complexity by sampling increasing numbers of reads (in increments of 100,000) and counting the number of unique peaks (>1 reads) and RefSeq transcripts (>10 reads) detected (**Fig S1B**). Reads corresponding to TSS peaks were then normalized to correct for library size (TPM, tags per million), and peaks with low expression (< 25% of the mean TPM expression per transcript) were filtered out. After normalization and filtering of non-reproducible and low-expression peaks, TSS clusters were defined using a sliding window approach with a window size of 5 nt. The beginning of a TSS cluster was defined as the position where the first TSS peak was encountered, and the cluster is extended until there were no longer TSS peaks within the span of the window. Since differences in 5'UTR length may be more impactful for short 5'UTR isoforms than for long ones (e.g. a 30 nt vs. a 45 nt 5'UTR may have quite different translation efficiencies due to the difference in length, but the difference between a 215 nt vs. a 200 nt 5'UTR may not have the similar implications), the size of the sliding window increased as the length of the 5'UTR increased, being scaled to be 2.5% of the length of the longest isoform for 5'UTRs longer than 200 nt. After TSS clusters were defined in each condition, overlapping clusters were unified between conditions to allow differential analysis of 5'UTR isoform expression. Once clusters were defined, reproducible and expression-filtered TSS

peaks within cluster regions were quantified for each sample to generate a counts table for further analysis.

To assess differential expression of 5'UTR isoforms detected in both conditions ("quantitative" differences) and all replicates, TSS cluster counts were normalized using the "voom" function from the limma R package[75]. Significant changes in the relative expression of 5'UTRs isoforms between conditions were then identified using per-gene linear models with the design:

$$Ex_{nano} \sim \gamma_I + \gamma_c + \gamma_R + \gamma_I * \gamma_c + \varepsilon$$

where $\boldsymbol{Ex_{nano}}$ is the expression for each 5'UTR isoform across all conditions and replicates, $\boldsymbol{\gamma_I}$ denotes relationship with 5'UTR isoform, $\boldsymbol{\gamma_c}$ is the relationship to the experimental condition, $\boldsymbol{\gamma_R}$ is relationship to replicate, $\boldsymbol{\gamma_I * \gamma_c}$ is the interaction between $\boldsymbol{\gamma_I}$ and $\boldsymbol{\gamma_c}$, and $\boldsymbol{\varepsilon}$ is the residual error. Similar to Anota2seq[31], a random variance model was then applied[83]. A low p-value for the $\boldsymbol{\gamma_I * \gamma_c}$ interaction term indicates a significant difference in 5'UTR isoform expression depending on condition, and is independent of changes in overall transcript expression or replicate effects. When 5'UTR isoforms were not detected in all samples, the regression-based approach used for detecting the quantitative differences was not appropriate. Instead, a "qualitative" approach was used. For 5'UTR isoforms that were not detected in all samples, but were detected in at least two replicates in both conditions, a Fisher's exact test was used to determine if there was a significant difference in expression of the 5'UTR isoform relative to all other isoforms between conditions (using the sums of nanocage sequencing reads per condition across all replicates). Finally, for a 5'UTR isoform that was only detected in one condition, Fisher's exact test is not applicable, and significance was assessed using probabilities. In the condition expressing the unique 5'UTR isoform the probability of expressing the shared isoforms relative to all isoforms was first calculated. In the condition not expressing the unique isoform, the probability of expressing only the shared isoform was then calculated:

$$p_{sj} = \left(\frac{r_{si}}{r_{ui} + r_{si}}\right)^{r_{sj}}$$

where **r** is the number of nanoCAGE sequencing reads summed across all replicates, **s** denotes shared isoforms, **u** denotes the uniquely expressed isoform, **i** the condition expressing the unique isoform and **j** the condition only expressing shared isoforms (i.e. $r_{uj} = 0$).

All *p*-values from the different arms of the statistical analysis were collected and adjusted for multiple testing using the Benjamini-Hochberg method. Transcripts that underwent significant TSS switching under hypoxia treatment were considered to be those with an FDR < 0.15.

Changepoint analysis for Identification of hypoxia-enriched or depleted 5'UTR sequences

After identifying transcripts that underwent significant hypoxia-induced TSS switching using the approach describe above, we next determined more precisely which portions of the 5'UTR sequences were specifically enriched or depleted as a result of the TSS switching. For each transcript identified as undergoing significant TSS switching under hypoxia, data from all biological replicates in each condition were pooled and the cumulative percentage of TPM-normalized reads was calculated at each TSS position. The cumulative percentages per TSS position under control (normoxic or DMSO) conditions were then subtracted from those under treatment (hypoxic or C48) conditions to provide the difference in cumulative percentage of reads at each TSS position. Next, a changepoint algorithm was applied to identify the positions in the difference distributions where a change had occurred. This was implemented using the "cpt.mean" function from the changepoint R package[43] with the arguments penalty = "AIC", method = "SegNeigh", and Q = 3 to allow up to two changepoints to be identified. The longest 5'UTR isoform sequence for each transcript was then divided at the nucleotide positions defined by the changepoints to generate three sequence segments based on their enrichment or depletion as a result of hypoxia-induced TSS switching. The enrichment or depletion of a 5'UTR sequence segment was quantified as the difference in the proportion of total TSS peak expression between conditions. Transcripts were also assigned a metric we termed the "TSS switch score", defined as the maximum difference in expression for a 5'UTR sequence segment minus the minimum difference. Higher TSS switch scores are indicative of TSS switching resulting in a greater change in the availability of particular 5'UTR sequences under hypoxia.

For transcripts with significant TSS switching, the percentage of GC content of 5'UTR sequence segments identified as enriched or depleted under hypoxia by changepoint analysis was calculated and visualized using empirical cumulative distribution functions. Differences in GC content between hypoxia-enriched or depleted sequences were assessed using a Wilcoxon-Mann-Whitney test.

Smart-seq2 library preparation, sequencing, and data preprocessing

RNAseq libraries for total and polysome-associated mRNA fractions from T47D, H9, cells cultured under hypoxia (1% O_2) and normoxia (20% O_2) were prepared using the Smart-seq2 protocol as previously described[84]. RNA quantity and quality was assessed by Qubit (Life Technologies) and Bioanalyzer (Agilent Technologies), and 10 ng of RNA was used as input material. After pre-amplification PCR 70 pg of cDNA underwent tagmentation in a total volume of 20 µL using the Nextera XT Kit (Illumina). Sequencing was then performed at the SciLifeLab National Genomics Infrastructure (NGI, Sweden) facility using the NovaSeq6000 (NovaSeq Control Software 1.6.0/RTA v3.4.4) with a 50-base paired-end setup using the 'NovaSeqStandard' workflow and S1 flow cell. Bcl to fastQ conversion was carried out using bcl2fastq_v2.20.0.422 from the CASAVA software suite. The quality scale was Sanger/phred33/Illumina 1.8+.

Adapters were removed from RNAseq reads using bbduk.sh from the BBTools software suite (sourceforge.net/projects/bbmap/) (settings k = 13 ktrim = n useshortkmers = t mink = 5 qtrim = t trimq = 10 minlength = 25). Ribosomal RNA was also removed using bbduk.sh, with default settings. Reads were aligned to hg38 using HISAT2[68] (settings --no-mixed --no-discordant), and uniquely mapping reads were quantified using the featureCounts function from the RSubreads package[69] with RefSeq gene definitions and default settings.

Analysis of differential translation

Raw counts from protein-coding genes with at least one read across all samples were TMM normalized[85] and $\log_2$ transformed using the "voom" function[75] as implemented in the Anota2seq R package[31]. The reproducibility of data from hypoxia and normoxia-treated, and polysome-associated and cytosolic mRNA samples was assessed using Principle Component Analysis after filtering genes by variance to select those within the highest quartile of standard deviation across samples.

Changes in polysome-associated and cytosolic mRNA under hypoxia were analyzed using the Anota2seq algorithm[31] with the normalized count data. Batch effects were accounted for in the models by including sample replicates using the "batchVec" argument in Anota2seq. Default threshold settings were used [minSlopeTranslation = -1, maxSlopeTranslation = 2, minSlopeBuffering = -2, maxSlopeBuffering = 1, deltaPT = deltaP = deltaTP = deltaT = log2(1.2)] with a significance threshold maxRvmPAdj = 0.15 (corresponding to an FDR < 0.15). Transcripts were classified into three modes of regulation (changes in mRNA abundance, changes in translation efficiency, and translational offsetting) using the "anota2seqRegModes' function.

Translatome modeling with Anota2seqUtils

The translatome modeling performed required two inputs; the per-gene fold changes in translation efficiency or offsetting between hypoxia and normoxia that were found to be significant using Anota2seq (described above), and a list of signatures describing regulatory variables for each gene. The Anota2seqUtils 'featureIntegration' function was used with arguments: regOnly = TRUE, regulationGen = 'translation' or 'buffering', allFeat = TRUE, useCorel = TRUE, analysis_type = 'lm', covarFilt = 10, NetModelSel = 'Omnibus'. Briefly, the software performs 3 steps. First, univariate linear models are used to identify significant associations between translational efficiency and individual variables. In the second step, a step-wise regression is performed beginning with the variable that was best able to explain the changes in translational efficiency from step 1. Variables are added iteratively, discarding those that do not improve the ability of the model to explain additional variance in translational efficiencies. This step both ranks the variables by importance and reveals covariance between them. In the final step, the covariance is removed to assess the adjusted contribution of each variable to the translational changes. This also allows calculation of the percent of variance in translation or offsetting explained by a given variable, adjusted for all other variables.

For the analysis presented in **Figs 2D-E and S3A-D**, the 5'UTR sequence corresponding to the mostly highly expressed isoform detected by nanoCAGE sequencing in the hypoxia condition was extracted. These sequences were used to define sets of mRNA feature variables that may be able to explain the translational regulation observed. These included characteristics such as the GC content, length, the presence and Kozak context of uORFs, and presence of polypurine motifs (defined as 6 consecutive purines). Folding energy was also calculated using the Mfold algorithm[86], and *de novo* 5'UTR motifs over-represented in regulated transcripts under hypoxia were identified using STREME[87]. G-quadruplexes were predicted using pqsfinder[88] (v1.10.1) with a min_score = 47, and TOP motifs were quantified using the TOPscore method described by Philippe et al.[24] using all reproducibly detected 5'UTR isoforms for a given transcript in the hypoxia condition. The presence of an additional set of evidence-supported RNA binding protein (RBP) motifs obtained from the ATtRACT database[89] was also quantified in 5'UTRs of transcripts that were regulated by translation or offsetting. Motifs were selected for inclusion in the final modeling using the 'featureIntegration' function of Anota2seqUtils (contrastSel = 1, regOnly = T, regulationGen = 'translation' or 'buffering', allFeat = TRUE, analysis_type = 'lm') to perform the same step-wise regression modeling described above, but only using the RBP motifs as variables to explain changes in translation or offsetting. Motifs that were significant in independently explaining proportions of the variance in translational changes were included in the final variable list.

For the analysis presented in **Figs 3I-L and S4A-B** additional variables describing how 5'UTR features change as a result of TSS switching were also added to the models. These included the change in weighted mean 5'UTR length (as both the actual difference in $\log_2$ length, and as categorical values i.e., no change, shorter, longer, as it was not clear that a larger change in 5'UTR length would necessarily have a greater regulatory impact than a smaller one), the difference in weighted mean GC content and folding energy, and the change in TOPscore between transcripts in hypoxia and normoxia. Finally, the TSS switch scores for each transcript from the changepoint analysis were also added to the list of variables.

All of the translatome models also included known signatures of translational regulation by various genes and pathways, including mTOR-sensitive translation and offsetting[38], ISR-sensitive translation[47,90], translation activated upon high eIF4E expression[91], translation suppressed upon KD of eIF4A1[41], U34-modified tRNA-dependent offsetting[57], DHX9-dependent translation[40], SNAT2-dependent translation[92], and high p-eIF4E-dependent translation[37]. Additional signatures of eIF4G[35] (GSE11011), DAP5[34] (GSE115142), and mTOR-dependent[38] (GSE76766) translation were obtained from supplemental material in published studies or following Anota2seq analysis.

Gene ontology enrichment analysis

Gene ontology enrichment analysis was performed using the Cytoscape (v.3.8.2.)[70] plug-in ClueGO (v.2.5.8)[71] with genes identified by Anota2seq analysis as regulated via "translation", mRNA abundance", and "buffering" in response to hypoxia treatment in T47D and H9 cell lines. The background for each cell line was defined as all genes passing expression thresholds described above for Anota2seq. Enrichments were selected based on the following criteria: *FDR* cutoff = 0.05, Correction Method Used = Benjamini-Hochberg, Statistical Test Used = Enrichment (Right-sided hypergeometric test), Kappa= 0.4, Min. Percentage = 10, Min GO Level = 3, Max GO Level = 8, Number of Genes = 5, GO Fusion = false, GO Group = true, Over View Term = SmallestPValue, Group By Kapp Statistics = true, Initial Group Size = 1, Sharing Group Percentage = 50.0, Ontology Used = GO_BiologicalProcess-EBI-UniProt-GOA-ACAP, Evidence codes used = All, Identifiers used = SymbolID.

Immunoblot analysis

Cells were placed on ice, washed with ice-cold PBS, lysed in RIPA buffer containing 1x Halt™ Protease and Phosphatase Inhibitor and cleared by centrifugation at 17,000 x g. Lysates for histone immunoblots were also sonicated (one pulse, 50% amplitude) prior to centrifugation. Protein concentration was determined with a Micro BCA™ Protein

Assay Kit as per manufacturer's instructions and read on a Spectramax ABS plus plate reader.
Equal amounts of protein were separated by polyacrylamide gel electrophoresis and transferred onto a 0.45µm nitrocellulose membrane (BioRad). Membranes were blocked with Odyssey blocking buffer, incubated with primary antibody in Odyssey Antibody dilution buffer over night at 4°C, washed in TBST, incubated with secondary antibody (IRDye 800CW or IRDye 680RD) matching the primary antibody species for 1h at room temperature and analysed on a LI-COR Odyssey CLx imaging system. Intensity of the bands was quantified with ImageStudio software.

In vitro *transcription*

pKS-FF-HCV-Ren plasmids containing the 5'UTR isoforms of PDK1 were linearized by *BamH*I digestion and purified by standard phenol/chloroform extraction. *In vitro* transcription and capping was carried out using a modified protocol from Steinberger et al.[64]. In short, 3 µg linearized plasmid was transcribed with 10 µl T3 RNA polymerase (NEB, M0378), 1× RNA polymerase buffer (NEB), 1 mM CTP, 1 mM ATP, 1 mM UTP, 0.2 mM GTP, 1 mM 3′-*O*-Me-^{m7}GpppG (Anti-Reverse Cap Analog [ARCA]; NEB, S1411), 100 U RNase Inhibitor (NEB, M0307) in a volume of 100 µL for 3 h at 37°C. 2.5 µL DNaseI (5U, NEB, M0303) was then added, and samples were incubated for an additional 30 min at 37°C. Samples were purified with the Invitrogen MegaClear kit according to the manufacturer's instructions. RNA was quantified using a Nanodrop, aliquoted and stored at −80°C.

In cell *translation experiments*

293T cells (1.6×10^5 per well) were seeded in 24-well plates. After 24 h cells were washed with serum-free media and then a mix of 150 ng *in vitro* transcribed RNA and 1 µL DMRIE-C reagent (Invitrogen, Cat#10459014) in 200 µL Opti-MEM was added directly to the cells as per manufacturer's instructions. After 1 h incubation (37°C, 5% CO_2) 200 µL DMEM 10% FBS containing Thapsigargin or INK128 was added to the cells to a final concentration of 400 nM or 50 nM, respectively. Media containing an equal volume of DMSO was used as vehicle control. After additional 7 h incubation time cells were washed with PBS and lysed using 100 µL Passive Lysis Buffer (Promega).

For translation experiments under hypoxia, 293T cells ($2x10^4$) were seeded in 24-well plates. After 24 h media was changed to fresh DMEM 10% FBS and cells were exposed to normoxia or hypoxia (0.5% O_2) for 24 h as described above. Cells were then washed with serum-free media and a mix of 150 ng *in vitro* transcribed RNA and 1 µL DMRIE-C reagent in 200 µl Opti-MEM was added directly to the cells. After 1 h incubation in

normoxia or hypoxia 200 µL DMEM 10% FBS was added to the cells. After additional 7 h incubation time in normoxia or hypoxia cells were washed with PBS and lysed using 100 µL Passive Lysis Buffer.

20 µL lysate was analyzed in with the Dual Luciferase kit (Promega) as per manufacturer's instructions on a GloMaxO Navigator Luminometer. Transfections were performed in duplicates and each sample was then analysed in duplicate.

Quantification and statistical analysis

Methods for quantification and statistics are described in detail in above sections, or in corresponding figure captions.

DATA AND CODE AVAILABILITY

Raw and processed RNA-seq, ChIP-seq, and nanoCAGE data have been deposited in the NCBI GEO database, with the accession number listed in the key resources table. All other raw datasets used in this study are listed in the key resources table.

All original code produced for the study is available on a Github repository. DOIs are listed in the key resources table.

Any additional information required to reproduce the analyses reported in this study is available from the lead contact upon request.

ACKNOWLEDGEMENTS

The authors would like to thank Willian Hahn, David Root, and Jerry Pelletier for generously sharing plasmid constructs used in this work. The authors would also like to acknowledge technical help from Shannon McLaughlan and advice from David Papadopoli, as well as support from the National Genomics Infrastructure in Stockholm funded by Science for Life Laboratory, the Knut and Alice Wallenberg Foundation and the Swedish Research Council, and SNIC/Uppsala Multidisciplinary Center for Advanced Computational Science for assistance with massively parallel sequencing and access to the UPPMAX computational infrastructure. This project was supported by CIHR (PS-159541) and CIHR (PS-148615) awarded to LMP. Work carried out in the IT lab was funded by CIHR (PJT-451236). IT is supported by a Fonds de recherche du

Québec (FRQ-S) Senior Investigator award. Work carried out in the OL lab was supported by grants from the Swedish Research Council (2020-01665), the Swedish Cancer Society (22 2186), the Cancer Research Funds of Radiumhemmet (211222) and the Wallenberg Academy Fellow program to OL.

Author contributions

LMP, IT, and OL conceived and designed the study. BD, LL, PJ, SC, LM, KT, and RP performed experimental work. KW, BD, PJ, RP, LMP, OL, and IT performed analysis and interpreted the data. KS, KW, and OL developed computational methods used for the analysis of sequencing data. KW, BD, LMP, OL, and IT wrote the manuscript, with input from all authors.

Declaration of interests

The authors declare that they have no conflict of interest.

FIGURE CAPTIONS

Figure 1: Hypoxia-induced TSS switching results in extensive remodeling of 5'UTRs.
A) T47D (n = 3), and H9 (n = 4) cells were cultured under hypoxia (0.5% O_2) or normoxia (20% O_2). Total RNA was isolated and transcriptome-wide quantification of 5'UTR isoforms was carried out using nanoCAGE sequencing.
B) Heatmaps of overall expression of hypoxia-responsive transcripts from nanoCAGE sequencing of T47D and H9 cells. One replicate of T47D in normoxia was discarded due to being an outlier.
C) Weighted mean 5'UTR length for mRNA transcripts measured by nanoCAGE compared to RefSeq annotated 5'UTR length. Colour gradient indicates point density.
D-E) Histograms showing the number of TSS clusters per protein-coding transcript in hypoxia and normoxia in T47D (D) and H9 (E) cells.
F) Kernel density estimation FDR distributions for differential TSS usage between hypoxia and normoxia in T47D, and H9 cells. Increased density of low FDRs indicates a higher frequency of changes in relative 5'UTR isoform abundance.
G) Barplot indicating the proportions of protein-coding transcripts with significantly altered TSS usage between hypoxia and normoxia (FDR < 0.15) in T47D, and H9 cells.
H) An example of a transcript that undergoes significant quantitative hypoxia-induced TSS switching in T47D cells. The x-axis represents the distance to the AUG start codon, with the black bar denoting the RefSeq-annotated 5'UTR length. The TSS clusters between 75-114 nt is expressed in both conditions, but has significantly different usage under hypoxia. Positions of TSS clusters relative to the AUG start codon are indicated

below bar plots. The percentages of total transcript expression per condition made up by a particular 5'UTR isoform are indicated above barplots.

I) Same as **(H)**, but an example of a transcript with a significant qualitative hypoxia-induced TSS change in T47D cells. The TSS cluster between 27-37 nt is expressed only under normoxic conditions.

J) Pie charts indicating the proportions of transcripts with changes in 5'UTR isoform abundance (due to TSS switching, from **G**) that have significantly (FDR < 0.15) increased (up), decreased (down), or unchanged overall expression between hypoxia and normoxia in T47D and H9 cells.

Figure 2: 5'UTR and translational machinery remodeling are coordinated under hypoxia.

A) Polysome tracing and global translation change in hypoxia-treated T47D cells compared to normoxia. Polysome-associated mRNA are considered those associated with >3 ribosomes. Global change in translation quantified as the ratio between the area under the curve for polysomes and 80S monosomes in each condition (n = 4).

B) Immunoblots of 4E-BP, eIF2α phosphorylation, and CyclinD from T47D cells in normoxia and hypoxia. 4E-BP1, eIF2α, and tubulin as loading controls, and HIF1α as a positive control for hypoxia.

C) Scatter plot of polysome-associated mRNA vs. total mRNA $\log_2$ fold changes in T47D cells (hypoxia vs. normoxia). Genes are colored according to their mode of regulation assigned by the Anota2seq algorithm (FDR < 0.15). The number of regulated mRNAs in each category is indicated in corresponding colors.

D) The relationship between known signatures of genes translationally regulated downstream of different pathways, and mRNA features of 5'UTRs characterized using nanoCAGE sequencing in hypoxia-treated T47D cells was analyzed using stepwise regression modeling. Network plot indicates the percentage of hypoxia-dependent translation changes in T47D cells that can be independently explained by each feature that was significant in the final regression model. Connections between features indicate significant correlations. Colors of the nodes indicate if the feature is associated with translation activation or suppression under hypoxia.

E) Same analysis as **D,** but examining the impact of pathways and 5'UTR features on translational offsetting induced by hypoxia in T47D cells.

F) Scatterplots comparing 5'UTR mRNA features that were significant in the model in **D** that can independently explain proportions of variance in translation, vs. the change in translation efficiency that occurs under hypoxia. Pearson's correlation coefficient and p-values indicated.

G) Same analysis as **F** but modeling features associated with translational offsetting under hypoxia (**E**).

Figure 3: TSS switching contributes to translational reprogramming under hypoxia.

A-D) An example of how changepoint analysis was used to identify specific 5'UTR sequence regions in NM_000387 that are enriched for, or depleted as a result of hypoxia-induced TSS switching seen in (**A**). Changepoints define 5'UTR sequence windows with differential enrichment or depletion under hypoxia (**B**). The degree of isoform switching can be scored by taking the difference in isoform expression between the most enriched and most depleted sequence windows (TSS switch score) (**C**), demonstrating a large difference in isoform expression, even in the absence of changes in overall transcript levels (**D**).

E) Kernel density estimation changepoint TSS switch score distributions for transcripts that undergo significant (FDR < 0.15) TSS switching under hypoxia in T47D (n = 2,552) and H9 (n = 3,423) cells. Shifts towards higher values indicate a greater degree of 5'UTR isoform relative abundance differences between hypoxia and normoxia.

F) Barplot of categories of 5'UTR sequences enriched under hypoxia identified by changepoint analysis. In T47D hypoxia-enriched sequences are most likely to represent extremes in 5'UTR length (either the longest isoforms, or the shortest), while TSS switching in H9 cells largely results in enrichment of longer 5'UTR isoforms.

G-H) Empirical cumulative distribution function plots comparing the percentage of GC content between hypoxia-enriched and depleted 5'UTR sequence windows identified by changepoint analysis in T47D cells. Left panel shows differences for transcripts with more modest differences in isoform abundance resulting from TSS switching (TSS switch score > 15), right panel shows differences for transcripts with larger isoform abundance differences (TSS switch score > 50). Differences shown for T47D (**G**) and H9 (**H**) cells.

I) Same analysis as in figure **2E**, with the addition of feature signatures quantifying TSS switching and hypoxia-induced changes to 5'UTRs. Features in the final regression model describing 5'UTR changes resulting from TSS switching are highlighted in bold.

J) Same analysis as in figure **I** but modeling changes in translational offsetting under hypoxia.

K) Scatterplots comparing signatures of TSS switching altering 5'UTRs that were significant in the model in **I** that can independently explain proportions of variance in translation, vs. the change in translation efficiency that occurs under hypoxia. Pearson's correlation coefficient and p-values indicated.

L) Signatures of TSS switching altering 5'UTRs that were significant in explaining proportions of variance in offsetting in the model in **J**.

Figure 4: TSS switching orchestrates adaptation to hypoxia by regulating mRNA isoform availability and translation.

A) Gene Ontology enrichments for biological processes for genes that undergo significant TSS switching leading to altered potential for translational regulation under hypoxia in T47D and H9 cells.
B) Quantification of 5'UTR isoforms for NM_001278549 (PDK1) in hypoxia and normoxia-treated T47D cells using nanoCAGE sequencing. Sequence windows defined by changepoints indicated by vertical orange lines. The lengths of PDK1 5'UTR isoforms that could be detected by 5'RACE in hypoxia-treated T47D cells are indicated by black bars in the hypoxia condition. Barplots indicate differences in relative expression of each TSS cluster between hypoxia and normoxia, and the overall expression of the transcript in both conditions. Numbers above barplots indicate the percentage of total transcript expression made up by that isoform, and numbers below indicate the nucleotide positions that define the TSS clusters.
C) Immunoblot showing induction of PDK1 and PDH phosphorylation (S323 and 293) with increased time under hypoxia treatment in T47D cells, and HIF1 as a positive control for hypoxia.
D) Changepoint analysis of NM_001278549 identifies changepoints at positions 36 and 87 nucleotides upstream of the start codon (right panel), which define shorter sequence windows with isoforms that are enriched under hypoxia and a longer window that is depleted (right panel).
E) Quantification of PDK1 5'UTR isoform expression in hypoxia and normoxia-treated T47D cells using RT-qPCR. P-value shown for the isoform:treatment interaction from the linear model with the design: % Isoform Expression ~ Replicate + Isoform + Treatment + Isoform:Treatment.
F) Polysome occupancy of PDK1 5'UTR isoforms under hypoxia and normoxia. RNA was isolated from each gradient fraction (bound by grey vertical lines) separated by polysome fractionation and subjected to RT-qPCR. The proportion of PDK1 5'UTR isoforms measured by RT-qPCR in each fraction is indicated by the blue (hypoxia) and red dashed (normoxia) lines, where the sum of all fractions for each mRNA is set to 100. The locations of 40S, 60S and 80S peaks are indicated. Shown is a representative plot of 1 of 3 replicates.
G) Top panel: Schematic of m7G-capped bicistronic reporter mRNA harbouring the 5'UTR of PDK1 (134, 57 or 36 nt) or the 5'UTR of beta-actin or ATF4 upstream of the firefly luciferase (FLuc) ORF and HCV IRES upstream of Renilla luciferase (Rluc) ORF. Bottom panel: Firefly luciferase values relative to Renilla luciferase in normoxia and hypoxia treated 293T cells transfected with the reporter mRNA. P-values are provided for differences between translation of isoforms, differences depending on treatment, and the interaction between isoform:treatment from the linear model with the design log2(Luminescence) ~ Replicate + Isoform + Treatment + Isoform:Treatment.
H) Firefly luciferase values relative to Renilla luciferase in DMSO, Thapsigargin (TG, 400 nM) and INK128 (INK, 50 nM) treated 293T transfected with the reporter mRNA

containing PDK1 5'UTR isoforms. P-values are provided for the linear model with the same design as (**G**).

Figure 5: Epigenomic alterations govern translation-regulating TSS selection.
A) Changes in the distribution of the H3K4me3 marks at TSS were detected using a Kolmorogov-Smirnov test. The proportion of TSSs for protein-coding genes with significant changes beyond a threshold of FDR < 0.01 are shown. N = 3 for both T47D and H9 cells, and the mean of the replicates was used in all comparisons.
B) An example of a gene where there is a significant change in the distribution (in this case, a broadening) of H3K4me3 around the TSS that is accompanied by TSS switching under hypoxia in T47D cells. The left panel shows the empirical cumulative distribution functions for the H3K4me3 read distributions shown in the right panel. The Wilcoxon and Kolmogorov-Smirnov p-values are indicated, as well as the directionality and magnitude of the shifts in the distribution at the quartiles.
C) Significant directional shifts in H3K4me3 distributions detected by two-tailed Wilcoxon signed-rank test. The proportion of TSSs for protein-coding genes with significant changes beyond a threshold of FDR < 0.01 are shown. N = 3 for both T47D and H9 cells, and the mean of the replicates was used in all comparisons.
D) Same as B, but an example of a gene with a strong directional shift in H3K4me3 distribution around the TSS where the distribution of the histone mark is extended downstream of the TSS in hypoxia-treated T47D cells.
E-F) Immunoblots of accumulation of H3K4me3 with C48 and hypoxia treatments. H3, and □-tubulin as a loading control, and HIF1□ as a positive control for hypoxia.
G) Kernel density estimation FDR distributions for differential TSS usage between C48 and DMSO-treated T47D cells indicating that TSS switching is induced by accumulation of H3K4me3.
H) Kernel density estimation changepoint TSS switch score distributions for transcripts that undergo significant (FDR < 0.15) TSS switching after C48 treatment (n = 974), compared to hypoxia treatment in T47D cells (n = 2,552) shifts towards higher values indicate a greater degree of 5'UTR isoform expression differences.
I) More significant TSS switching events under hypoxia are more likely to the be recapitulated by C48 treatment. The FDR distribution for TSS switching under hypoxia was divided into deciles and the proportion of equivalent changes in 5'UTR isoforms between hypoxia vs. normoxia and C48 vs. DMSO comparisons was quantified. The dashed horizontal line marks the proportion of changes that could be expected to be the same by chance (20.6%, derived from Monte Carlo simulation), P-value and Spearman's rho indicated.
J) By comparing the 5'UTR sequence window enrichments from the changepoint analysis of transcripts with significant TSS switching under hypoxia to the changes that occurred following C48 treatment, a subset of 477 transcripts were identified that

underwent the same changes in 5'UTR isoform expression. Pie chart indicates the proportions of these transcripts that have significantly (FDR < 0.15) increased (up), decreased (down), or unchanged overall expression between hypoxia and normoxia in T47D, indicative of transcriptional activation or suppression or altered stability.

K) Empirical cumulative distribution functions (top panel) for the H3K4me3 read distributions around the PLOD2 TSS (bottom panel) in hypoxia and normoxia-treated T47D cells.

L) Quantification of 5'UTR isoforms of PLOD2 in hypoxia and normoxia-treated (left), and C48 and DMSO-treated T47D cells (right) using nanoCAGE sequencing.

M) Changepoint analysis of the 5'UTR isoform changes in **L**, identifying enriched and depleted 5'UTR sequence windows in both treatment comparisons. Barplots show changes in overall transcript expression between treatments in T47D cells (n = 4 for each treatment condition).

SUPPLEMENTAL FIGURE CAPTIONS

Figure S1. Related to Figure 1: Preprocessing and quality control of nanoCAGE sequencing.

A) Summary of preprocessing of nanoCAGE sequencing data including removal of adapters, duplicate reads, ribosomal RNA, and reads not mapping to 5'UTR regions.

B) NanoCAGE sequencing library complexity for T47D, and H9 cells evaluated according to the number of distinct peaks (TSSs) and protein-coding transcripts (RefSeq) detected with increasing numbers of sampled sequencing reads.

C) Principle component analysis of 5'UTR isoform expression in T47D, and H9 cells grown in hypoxia and normoxia quantified by nanoCAGE.

Figure S2. Related to Figure 2: 5'UTR and translational machinery remodeling are coordinated under hypoxia.

A) Polysome tracing and global translation change in hypoxia-treated H9 cells compared to normoxia controls. Polysome-associated mRNA are considered those with >3 ribosomes. Global change in translation quantified as the ratio between the area under the curve for polysomes and the 80S in each condition (n = 3).

B) Immunoblots of rpS6, 4E-BP, and eIF2α phosphorylation from H9 cells in normoxia and hypoxia. 4E-BP1, rpS6, eIF2α, and β-actin loading controls, and HIF1□ as a positive control for hypoxia.

C) Scatter plot of polysome-associated mRNA vs. total mRNA $\log_2$ fold changes in H9 cells (hypoxia vs. normoxia). Genes are colored according to their mode of regulation assigned by the Anota2seq algorithm (FDR < 0.15). The number of regulated mRNAs in each category are indicated in corresponding colors.

D) Gene Ontology enrichments for biological processes for gene sets assigned to each regulatory mode in **Fig 2C** for T47D cells.
E) Gene Ontology enrichments for biological processes for gene sets assigned to each regulatory mode in **S2C** for H9 cells.
F-G) Scatterplots from Anota2seq translatome analysis of T47D (**F**) and H9 cells (**G**) with the location of canonical TOP mRNAs from Philippe et al.[24] colored (left panels). Empirical cumulative distribution functions showing the $\log_2$ fold changes for the TOP mRNAs in polysome-associated (middle panels), and total mRNA fractions (right panels). Grey lines correspond to the background of all non-TOP genes. Significant differences between destitutions determined by Wilcoxan rank-sum test. Differences in distributions at quantiles indicated.

Figure S3. Related to Figure 2: 5'UTR and translational machinery remodeling are coordinated under hypoxia.
A) The relationship between known signatures of genes translationally regulated downstream of different pathways, and mRNA features of 5'UTRs characterized using nanoCAGE sequencing in hypoxia-treated H9 cells was analyzed using stepwise regression modeling. Network plot indicates the percentage of hypoxia-dependent translation changes in H9 cells that can be independently explained by each feature that was significant in the final regression model. Connections between features indicates significant correlations. Colors of the nodes indicate if the feature is associated with translation activation or suppression under hypoxia.
B) Same analysis as **A,** but examining the impact of pathways and 5'UTR features on translational offsetting induced by hypoxia in H9 cells.
C) Scatterplots comparing 5'UTR mRNA features that were significant in the model in **A** that can independently explain proportions of variance in translation, vs. the change in translation efficiency that occurs under hypoxia. Pearson's correlation coefficient and p-values indicated.
D) Same analysis as **B** but modeling features associated with translational offsetting under hypoxia.

Figure S4. Related to Figure 3: TSS switching contributes to translational reprogramming under hypoxia.
A) Same analysis as in figure **S3B**, with the addition of feature signatures quantifying TSS switching and hypoxia-induced changes to 5'UTRs in H9 cells. Features in the final regression model describing 5'UTR changes are highlighted in bold.
B) Scatterplots comparing signatures of TSS switching altering 5'UTRs that were significant in the model in **A** that can independently explain proportions of variance in translation, vs. the change in translation efficiency that occurs under hypoxia. Pearson's correlation coefficient and p-values indicated.

Figure S5. Related to Figure 4: TSS switching orchestrates adaptation to hypoxia by regulating mRNA isoform availability and translation.

A) Quantification of 5'UTR isoforms for NM_001278549 (PDK1) in hypoxia and normoxia-treated H9 cells using nanoCAGE sequencing. Sequence windows defined by changepoints indicated by vertical orange lines. Barplots indicate differences in relative expression of each TSS cluster between hypoxia and normoxia, and the overall expression of the transcript in both conditions. Numbers above barplots indicate the percentage of total transcript expression made up by that isoform, and numbers below indicate the nucleotide positions that define the TSS clusters.

B) Immunoblots of rpS6, 4E-BP, eIF2α phosphorylation and PDK1 from T47D cells used in polysome profiling in normoxia and hypoxia. 4E-BP1, rpS6, eIF2α, loading controls.

C) Changepoint analysis of NM_001278549 identified changepoints at positions 24 and 97 nucleotides upstream of the start codon (right panel), which define shorter sequence windows with isoforms that are enriched under hypoxia and a longer window that is depleted (right panel).

Figure S6. Epigenomic alterations govern translation-regulating TSS selection.

A) Principle component analysis of changes in H3K4me3 peaks surrounding TSSs T47D, and H9 cells grown in hypoxia and normoxia and quantified by ChIPseq (n = 3).

B) Immunoblots of H3K4me3, H3, and rpS6 and eIF2α phosphorylation, with □-tubulin as a loading control, demonstrating H3K4me3 accumulation with increasing doses of C48.

C) Principle component analysis of 5'UTR isoform expression in T47D cells treated with 10 uM C48 or DMSO and quantified by nanoCAGE sequencing.

D) Kernel density estimation FDR distributions for differential transcript expression between C48 and DMSO in T47D cells, evaluated using DESeq2. C48 treatment induces essentially no changes in transcription.

E) Same as in **D** examining differential transcript expression between hypoxia and normoxia treated T47D cells. Increased density of low FDRs indicates a higher frequency of changes in transcript abundance.

F) Changepoint analysis of NM_001278549 (PDK1) identifies changepoints at positions 72 and 87 nucleotides upstream of the start codon.

G-H) Plots showing association of between TSS switch score and $\log_2$ fold change in overall transcript abundance between hypoxia and normoxia for T47D (**G**) and H9 cells (**H**). R^2 values and p-values for Pearson correlations indicated.

REFERENCES

1. Quail, D.F., Taylor, M.J., and Postovit, L.-M. (2012). Microenvironmental regulation of cancer stem cell phenotypes. Curr Stem Cell Res Ther *7*, 197–216. 10.2174/157488812799859838.

2. Conley, S.J., Gheordunescu, E., Kakarala, P., Newman, B., Korkaya, H., Heath, A.N., Clouthier, S.G., and Wicha, M.S. (2012). Antiangiogenic agents increase breast cancer stem cells via the generation of tumor hypoxia. Proceedings of the National Academy of Sciences *109*, 2784–2789. 10.1073/pnas.1018866109.

3. Lee, L.J., Papadopoli, D., Jewer, M., Rincon, S. del, Topisirovic, I., Lawrence, M.G., and Postovit, L.-M. (2021). Cancer Plasticity: The Role of mRNA Translation. Trends in Cancer *7*, 134–145. 10.1016/j.trecan.2020.09.005.

4. Kenneth, N.S., and Rocha, S. (2008). Regulation of gene expression by hypoxia. Biochemical Journal *414*, 19–29. 10.1042/BJ20081055.

5. Wouters, B.G., and Koritzinsky, M. (2008). Hypoxia signalling through mTOR and the unfolded protein response in cancer. Nat Rev Cancer *8*, 851–864. 10.1038/nrc2501.

6. Batie, M., Frost, J., Frost, M., Wilson, J.W., Schofield, P., and Rocha, S. (2019). Hypoxia induces rapid changes to histone methylation and reprograms chromatin. Science *363*, 1222–1226. 10.1126/science.aau5870.

7. Chakraborty, A.A., Laukka, T., Myllykoski, M., Ringel, A.E., Booker, M.A., Tolstorukov, M.Y., Meng, Y.J., Meier, S.R., Jennings, R.B., Creech, A.L., et al.

(2019). Histone demethylase KDM6A directly senses oxygen to control chromatin and cell fate. Science *363*, 1217–1222. 10.1126/science.aaw1026.

8. Millán-Zambrano, G., Burton, A., Bannister, A.J., and Schneider, R. (2022). Histone post-translational modifications — cause and consequence of genome function. Nat Rev Genet *23*, 563–580. 10.1038/s41576-022-00468-7.

9. Santos-Rosa, H., Schneider, R., Bannister, A.J., Sherriff, J., Bernstein, B.E., Emre, N.C.T., Schreiber, S.L., Mellor, J., and Kouzarides, T. (2002). Active genes are tri-methylated at K4 of histone H3. Nature *419*, 407–411. 10.1038/nature01080.

10. Guenther, M.G., Levine, S.S., Boyer, L.A., Jaenisch, R., and Young, R.A. (2007). A Chromatin Landmark and Transcription Initiation at Most Promoters in Human Cells. Cell *130*, 77–88. 10.1016/j.cell.2007.05.042.

11. Benayoun, B.A., Pollina, E.A., Ucar, D., Mahmoudi, S., Karra, K., Wong, E.D., Devarajan, K., Daugherty, A.C., Kundaje, A.B., Mancini, E., et al. (2014). H3K4me3 Breadth Is Linked to Cell Identity and Transcriptional Consistency. Cell *158*, 673–688. 10.1016/j.cell.2014.06.027.

12. Howe, F.S., Fischl, H., Murray, S.C., and Mellor, J. (2017). Is H3K4me3 instructive for transcription activation? BioEssays *39*, e201600095. 10.1002/bies.201600095.

13. Pollard, P.J., Loenarz, C., Mole, D.R., McDonough, M.A., Gleadle, J.M., Schofield, C.J., and Ratcliffe, P.J. (2008). Regulation of Jumonji-domain-containing histone demethylases by hypoxia-inducible factor (HIF)-1□. Biochem J *416*, 387–394. 10.1042/BJ20081238.

14. Wellmann, S., Bettkober, M., Zelmer, A., Seeger, K., Faigle, M., Eltzschig, H.K., and Bührer, C. (2008). Hypoxia upregulates the histone demethylase JMJD1A via HIF-1. Biochem Biophys Res Commun *372*, 892–897. 10.1016/j.bbrc.2008.05.150.

15. Beyer, S., Kristensen, M.M., Jensen, K.S., Johansen, J.V., and Staller, P. (2008). The histone demethylases JMJD1A and JMJD2B are transcriptional targets of hypoxia-inducible factor HIF. J Biol Chem *283*, 36542–36552. 10.1074/jbc.M804578200.

16. Hancock, R.L., Dunne, K., Walport, L.J., Flashman, E., and Kawamura, A. (2015). Epigenetic regulation by histone demethylases in hypoxia. Epigenomics *7*, 791–811. 10.2217/epi.15.24.

17. Buttgereit, F., and Brand, M.D. (1995). A hierarchy of ATP-consuming processes in mammalian cells. Biochem J *312*, 163–167.

18. Brugarolas, J., Lei, K., Hurley, R.L., Manning, B.D., Reiling, J.H., Hafen, E., Witters, L.A., Ellisen, L.W., and Kaelin, W.G. (2004). Regulation of mTOR function in response to hypoxia by REDD1 and the TSC1/TSC2 tumor suppressor complex. Genes Dev *18*, 2893–2904. 10.1101/gad.1256804.

19. Koumenis, C., Naczki, C., Koritzinsky, M., Rastani, S., Diehl, A., Sonenberg, N., Koromilas, A., and Wouters, B.G. (2002). Regulation of protein synthesis by hypoxia via activation of the endoplasmic reticulum kinase PERK and phosphorylation of the translation initiation factor eIF2□. Mol Cell Biol *22*, 7405–7416. 10.1128/MCB.22.21.7405-7416.2002.

20. Hinnebusch, A.G., Ivanov, I.P., and Sonenberg, N. (2016). Translational control by 5'-untranslated regions of eukaryotic mRNAs. Science *352*, 1413–1416. 10.1126/science.aad9868.

21. Guan, B.-J., van Hoef, V., Jobava, R., Elroy-Stein, O., Valasek, L.S., Cargnello, M., Gao, X.-H., Krokowski, D., Merrick, W.C., Kimball, S.R., et al. (2017). A Unique ISR Program Determines Cellular Responses to Chronic Stress. Mol Cell *68*, 885-900.e6. 10.1016/j.molcel.2017.11.007.

22. Gandin, V., Masvidal, L., Hulea, L., Gravel, S.-P., Cargnello, M., McLaughlan, S., Cai, Y., Balanathan, P., Morita, M., Rajakumar, A., et al. (2016). nanoCAGE reveals 5′ UTR features that define specific modes of translation of functionally related MTOR-sensitive mRNAs. Genome Res. *26*, 636–648. 10.1101/gr.197566.115.

23. Stolovich, M., Tang, H., Hornstein, E., Levy, G., Cohen, R., Bae, S.S., Birnbaum, M.J., and Meyuhas, O. (2002). Transduction of growth or mitogenic signals into translational activation of TOP mRNAs is fully reliant on the phosphatidylinositol 3-kinase-mediated pathway but requires neither S6K1 nor rpS6 phosphorylation. Mol Cell Biol *22*, 8101–8113. 10.1128/MCB.22.23.8101-8113.2002.

24. Philippe, L., van den Elzen, A.M.G., Watson, M.J., and Thoreen, C.C. (2020). Global analysis of LARP1 translation targets reveals tunable and dynamic features of 5′ TOP motifs. Proc Natl Acad Sci USA *117*, 5319–5328. 10.1073/pnas.1912864117.

25. Masvidal, L., Hulea, L., Furic, L., Topisirovic, I., and Larsson, O. (2017). mTOR-sensitive translation: Cleared fog reveals more trees. RNA Biol *14*, 1299–1305. 10.1080/15476286.2017.1290041.

26. Jewer, M., Lee, L., Leibovitch, M., Zhang, G., Liu, J., Findlay, S.D., Vincent, K.M., Tandoc, K., Dieters-Castator, D., Quail, D.F., et al. (2020). Translational control of breast cancer plasticity. Nat Commun *11*, 2498. 10.1038/s41467-020-16352-z.

27. Pelletier, J., and Sonenberg, N. (2019). The Organizing Principles of Eukaryotic Ribosome Recruitment. Annu Rev Biochem *88*, 307–335. 10.1146/annurev-biochem-013118-111042.

28. Ristau, J., Watt, K., Oertlin, C., and Larsson, O. (2022). Polysome Fractionation for Transcriptome-Wide Studies of mRNA TranslationMRNA translation. In Estrogen Receptors: Methods and Protocols Methods in Molecular Biology., K. M. Eyster, ed. (Springer US), pp. 223–241. 10.1007/978-1-0716-1920-9_14.

29. Warner, J.R., Knopf, P.M., and Rich, A. (1963). A multiple ribosomal structure in protein synthesis. Proc Natl Acad Sci U S A *49*, 122–129. 10.1073/pnas.49.1.122.

30. Dowling, R.J.O., Topisirovic, I., Alain, T., Bidinosti, M., Fonseca, B.D., Petroulakis, E., Wang, X., Larsson, O., Selvaraj, A., Liu, Y., et al. (2010). mTORC1-mediated cell proliferation, but not cell growth, controlled by the 4E-BPs. Science *328*, 1172–1176. 10.1126/science.1187532.

31. Oertlin, C., Lorent, J., Murie, C., Furic, L., Topisirovic, I., and Larsson, O. (2019). Generally applicable transcriptome-wide analysis of translation using anota2seq. Nucleic Acids Research *47*, e70–e70. 10.1093/nar/gkz223.

32. Kusnadi, E.P., Timpone, C., Topisirovic, I., Larsson, O., and Furic, L. (2022). Regulation of gene expression via translational buffering. Biochimica et Biophysica Acta (BBA) - Molecular Cell Research *1869*, 119140. 10.1016/j.bbamcr.2021.119140.

33. Volta, V., Pérez-Baos, S., de la Parra, C., Katsara, O., Ernlund, A., Dornbaum, S., and Schneider, R.J. (2021). A DAP5/eIF3d alternate mRNA translation mechanism promotes differentiation and immune suppression by human regulatory T cells. Nat Commun *12*, 6979. 10.1038/s41467-021-27087-w.

34. de la Parra, C., Ernlund, A., Alard, A., Ruggles, K., Ueberheide, B., and Schneider, R.J. (2018). A widespread alternate form of cap-dependent mRNA translation initiation. Nat Commun *9*, 3068. 10.1038/s41467-018-05539-0.

35. Ramírez-Valle, F., Braunstein, S., Zavadil, J., Formenti, S.C., and Schneider, R.J. (2008). eIF4GI links nutrient sensing by mTOR to cell proliferation and inhibition of autophagy. J Cell Biol *181*, 293–307. 10.1083/jcb.200710215.

36. Larsson, O., Li, S., Issaenko, O.A., Avdulov, S., Peterson, M., Smith, K., Bitterman, P.B., and Polunovsky, V.A. (2007). Eukaryotic translation initiation factor 4E induced progression of primary human mammary epithelial cells along the cancer pathway is associated with targeted translational deregulation of oncogenic drivers and inhibitors. Cancer Res *67*, 6814–6824. 10.1158/0008-5472.CAN-07-0752.

37. Karampelias, C., Watt, K., Mattsson, C.L., Ruiz, Á.F., Rezanejad, H., Mi, J., Liu, X., Chu, L., Locasale, J.W., Korbutt, G.S., et al. (2022). MNK2 deficiency potentiates β-cell regeneration via translational regulation. Nat Chem Biol *18*, 942–953. 10.1038/s41589-022-01047-x.

38. Gandin, V., Masvidal, L., Cargnello, M., Gyenis, L., McLaughlan, S., Cai, Y., Tenkerian, C., Morita, M., Balanathan, P., Jean-Jean, O., et al. (2016). mTORC1 and CK2 coordinate ternary and eIF4F complex assembly. Nat Commun *7*, 11127. 10.1038/ncomms11127.

39. Krokowski, D., Jobava, R., Szkop, K.J., Chen, C.-W., Fu, X., Venus, S., Guan, B.-J., Wu, J., Gao, Z., Banaszuk, W., et al. (2022). Stress-induced perturbations in

intracellular amino acids reprogram mRNA translation in osmoadaptation independently of the ISR. Cell Rep *40*, 111092. 10.1016/j.celrep.2022.111092.

40. Lee, T., Di Paola, D., Malina, A., Mills, J.R., Kreps, A., Grosse, F., Tang, H., Zannis-Hadjopoulos, M., Larsson, O., and Pelletier, J. (2014). Suppression of the DHX9 Helicase Induces Premature Senescence in Human Diploid Fibroblasts in a p53-dependent Manner. J Biol Chem *289*, 22798–22814. 10.1074/jbc.M114.568535.

41. Modelska, A., Turro, E., Russell, R., Beaton, J., Sbarrato, T., Spriggs, K., Miller, J., Gräf, S., Provenzano, E., Blows, F., et al. (2015). The malignant phenotype in breast cancer is driven by eIF4A1-mediated changes in the translational landscape. Cell Death Dis *6*, e1603–e1603. 10.1038/cddis.2014.542.

42. Lorent, J., Kusnadi, E.P., van Hoef, V., Rebello, R.J., Leibovitch, M., Ristau, J., Chen, S., Lawrence, M.G., Szkop, K.J., Samreen, B., et al. (2019). Translational offsetting as a mode of estrogen receptor α-dependent regulation of gene expression. The EMBO Journal *38*, e101323. 10.15252/embj.2018101323.

43. Killick, R., and Eckley, I.A. (2014). changepoint: An R Package for Changepoint Analysis. Journal of Statistical Software *58*, 1–19. 10.18637/jss.v058.i03.

44. Kim, J., Tchernyshyov, I., Semenza, G.L., and Dang, C.V. (2006). HIF-1-mediated expression of pyruvate dehydrogenase kinase: A metabolic switch required for cellular adaptation to hypoxia. Cell Metabolism *3*, 177–185. 10.1016/j.cmet.2006.02.002.

45. Patel, M.S., Nemeria, N.S., Furey, W., and Jordan, F. (2014). The pyruvate dehydrogenase complexes: structure-based function and regulation. J Biol Chem *289*, 16615–16623. 10.1074/jbc.R114.563148.

46. Ito, K., and Suda, T. (2014). Metabolic requirements for the maintenance of self-renewing stem cells. Nat Rev Mol Cell Biol *15*, 243–256. 10.1038/nrm3772.

47. Guan, B.-J., van Hoef, V., Jobava, R., Elroy-Stein, O., Valasek, L.S., Cargnello, M., Gao, X.-H., Krokowski, D., Merrick, W.C., Kimball, S.R., et al. (2017). A Unique ISR Program Determines Cellular Responses to Chronic Stress. Mol Cell *68*, 885-900.e6. 10.1016/j.molcel.2017.11.007.

48. Sugimoto, Y., and Ratcliffe, P.J. (2022). Isoform-resolved mRNA profiling of ribosome load defines interplay of HIF and mTOR dysregulation in kidney cancer. Nat Struct Mol Biol *29*, 871–880. 10.1038/s41594-022-00819-2.

49. Rosell-García, T., Palomo-Álvarez, O., and Rodríguez-Pascual, F. (2019). A hierarchical network of hypoxia-inducible factor and SMAD proteins governs procollagen lysyl hydroxylase 2 induction by hypoxia and transforming growth factor β1. J Biol Chem *294*, 14308–14318. 10.1074/jbc.RA119.007674.

50. Hofbauer, K.-H., Gess, B., Lohaus, C., Meyer, H.E., Katschinski, D., and Kurtz, A. (2003). Oxygen tension regulates the expression of a group of procollagen hydroxylases. European Journal of Biochemistry *270*, 4515–4522. 10.1046/j.1432-1033.2003.03846.x.

51. Lodish, H.F. (1974). Model for the regulation of mRNA translation applied to haemoglobin synthesis. Nature *251*, 385–388. 10.1038/251385a0.

52. FANTOM Consortium and the RIKEN PMI and CLST (DGT), Forrest, A.R.R., Kawaji, H., Rehli, M., Baillie, J.K., de Hoon, M.J.L., Haberle, V., Lassmann, T., Kulakovskiy, I.V., Lizio, M., et al. (2014). A promoter-level mammalian expression atlas. Nature *507*, 462–470. 10.1038/nature13182.

53. Haberle, V., Li, N., Hadzhiev, Y., Plessy, C., Previti, C., Nepal, C., Gehrig, J., Dong, X., Akalin, A., Suzuki, A.M., et al. (2014). Two independent transcription initiation codes overlap on vertebrate core promoters. Nature *507*, 381–385. 10.1038/nature12974.

54. Qamra, A., Xing, M., Padmanabhan, N., Kwok, J.J.T., Zhang, S., Xu, C., Leong, Y.S., Lee Lim, A.P., Tang, Q., Ooi, W.F., et al. (2017). Epigenomic Promoter Alterations Amplify Gene Isoform and Immunogenic Diversity in Gastric Adenocarcinoma. Cancer Discov *7*, 630–651. 10.1158/2159-8290.CD-16-1022.

55. Dieudonné, F.-X., O'Connor, P.B.F., Gubler-Jaquier, P., Yasrebi, H., Conne, B., Nikolaev, S., Antonarakis, S., Baranov, P.V., and Curran, J. (2015). The effect of heterogeneous Transcription Start Sites (TSS) on the translatome: implications for the mammalian cellular phenotype. BMC Genomics *16*, 986. 10.1186/s12864-015-2179-8.

56. Tsuchihara, K., Suzuki, Y., Wakaguri, H., Irie, T., Tanimoto, K., Hashimoto, S., Matsushima, K., Mizushima-Sugano, J., Yamashita, R., Nakai, K., et al. (2009). Massive transcriptional start site analysis of human genes in hypoxia cells. Nucleic Acids Res *37*, 2249–2263. 10.1093/nar/gkp066.

57. Lorent, J., Kusnadi, E.P., Hoef, V., Rebello, R.J., Leibovitch, M., Ristau, J., Chen, S., Lawrence, M.G., Szkop, K.J., Samreen, B., et al. (2019). Translational offsetting as a mode of estrogen receptor α-dependent regulation of gene expression. EMBO J *38*. 10.15252/embj.2018101323.

58. Hay, N. (2010). Mnk earmarks eIF4E for cancer therapy. Proceedings of the National Academy of Sciences *107*, 13975–13976. 10.1073/pnas.1008908107.

59. Vermeulen, M., Mulder, K.W., Denissov, S., Pijnappel, W.W.M.P., van Schaik, F.M.A., Varier, R.A., Baltissen, M.P.A., Stunnenberg, H.G., Mann, M., and Timmers, H.T.M. (2007). Selective anchoring of TFIID to nucleosomes by trimethylation of histone H3 lysine 4. Cell *131*, 58–69. 10.1016/j.cell.2007.08.016.

60. Cano-Rodriguez, D., Gjaltema, R.A.F., Jilderda, L.J., Jellema, P., Dokter-Fokkens, J., Ruiters, M.H.J., and Rots, M.G. (2016). Writing of H3K4Me3 overcomes epigenetic silencing in a sustained but context-dependent manner. Nat Commun *7*, 12284. 10.1038/ncomms12284.

61. Henikoff, S., and Shilatifard, A. (2011). Histone modification: cause or cog? Trends Genet *27*, 389–396. 10.1016/j.tig.2011.06.006.

62. Moore, C.E.J., Mikolajek, H., Regufe da Mota, S., Wang, X., Kenney, J.W., Werner, J.M., and Proud, C.G. (2015). Elongation Factor 2 Kinase Is Regulated by Proline Hydroxylation and Protects Cells during Hypoxia. Mol Cell Biol *35*, 1788–1804. 10.1128/MCB.01457-14.

63. Liu, S., Hausmann, S., Carlson, S.M., Fuentes, M.E., Francis, J.W., Pillai, R., Lofgren, S.M., Hulea, L., Tandoc, K., Lu, J., et al. (2019). METTL13 Methylation of eEF1A Increases Translational Output to Promote Tumorigenesis. Cell *176*, 491-504.e21. 10.1016/j.cell.2018.11.038.

64. Steinberger, J., Shen, L., J. Kiniry, S., Naineni, S.K., Cencic, R., Amiri, M., Aboushawareb, S.A.E., Chu, J., Maïga, R.I., Yachnin, B.J., et al. (2020). Identification and characterization of hippuristanol-resistant mutants reveals eIF4A1 dependencies within mRNA 5′ leader regions. Nucleic Acids Research *48*, 9521–9537. 10.1093/nar/gkaa662.

65. Johannessen, C.M., Boehm, J.S., Kim, S.Y., Thomas, S.R., Wardwell, L., Johnson, L.A., Emery, C.M., Stransky, N., Cogdill, A.P., Barretina, J., et al. (2010). COT drives resistance to RAF inhibition through MAP kinase pathway reactivation. Nature *468*, 968–972. 10.1038/nature09627.

66. Langmead, B., Trapnell, C., Pop, M., and Salzberg, S.L. (2009). Ultrafast and memory-efficient alignment of short DNA sequences to the human genome. Genome Biol *10*, R25. 10.1186/gb-2009-10-3-r25.

67. Quinlan, A.R., and Hall, I.M. (2010). BEDTools: a flexible suite of utilities for comparing genomic features. Bioinformatics *26*, 841–842. 10.1093/bioinformatics/btq033.

68. Kim, D., Paggi, J.M., Park, C., Bennett, C., and Salzberg, S.L. (2019). Graph-based genome alignment and genotyping with HISAT2 and HISAT-genotype. Nature Biotechnology *37*, 907–915. 10.1038/s41587-019-0201-4.

69. Liao, Y., Smyth, G.K., and Shi, W. (2014). featureCounts: an efficient general purpose program for assigning sequence reads to genomic features. Bioinformatics *30*, 923–930. 10.1093/bioinformatics/btt656.

70. Shannon, P., Markiel, A., Ozier, O., Baliga, N.S., Wang, J.T., Ramage, D., Amin, N., Schwikowski, B., and Ideker, T. (2003). Cytoscape: A Software Environment for

Integrated Models of Biomolecular Interaction Networks. Genome Res *13*, 2498–2504. 10.1101/gr.1239303.

71. Bindea, G., Mlecnik, B., Hackl, H., Charoentong, P., Tosolini, M., Kirilovsky, A., Fridman, W.-H., Pagès, F., Trajanoski, Z., and Galon, J. (2009). ClueGO: a Cytoscape plug-in to decipher functionally grouped gene ontology and pathway annotation networks. Bioinformatics *25*, 1091–1093. 10.1093/bioinformatics/btp101.

72. Lassmann, T. (2015). TagDust2: a generic method to extract reads from sequencing data. BMC Bioinformatics *16*, 24. 10.1186/s12859-015-0454-y.

73. Martin, M. (2011). Cutadapt removes adapter sequences from high-throughput sequencing reads. EMBnet.journal *17*, 10–12. 10.14806/ej.17.1.200.

74. Tang, D.T.P., Plessy, C., Salimullah, M., Suzuki, A.M., Calligaris, R., Gustincich, S., and Carninci, P. (2013). Suppression of artifacts and barcode bias in high-throughput transcriptome analyses utilizing template switching. Nucleic Acids Res *41*, e44. 10.1093/nar/gks1128.

75. Ritchie, M.E., Phipson, B., Wu, D., Hu, Y., Law, C.W., Shi, W., and Smyth, G.K. (2015). limma powers differential expression analyses for RNA-sequencing and microarray studies. Nucleic Acids Research *43*, e47–e47. 10.1093/nar/gkv007.

76. Love, M.I., Huber, W., and Anders, S. (2014). Moderated estimation of fold change and dispersion for RNA-seq data with DESeq2. Genome Biology *15*, 550. 10.1186/s13059-014-0550-8.

77. Wickham, H. (2016). ggplot2 (Springer International Publishing) 10.1007/978-3-319-24277-4.

78. Gandin, V., Sikström, K., Alain, T., Morita, M., McLaughlan, S., Larsson, O., and Topisirovic, I. (2014). Polysome Fractionation and Analysis of Mammalian Translatomes on a Genome-wide Scale. JoVE (Journal of Visualized Experiments), e51455. 10.3791/51455.

79. Shah, R.N., Grzybowski, A.T., Cornett, E.M., Johnstone, A.L., Dickson, B.M., Boone, B.A., Cheek, M.A., Cowles, M.W., Maryanski, D., Meiners, M.J., et al. (2018). Examining the Roles of H3K4 Methylation States with Systematically Characterized Antibodies. Mol Cell *72*, 162-177.e7. 10.1016/j.molcel.2018.08.015.

80. Ewels, P.A., Peltzer, A., Fillinger, S., Patel, H., Alneberg, J., Wilm, A., Garcia, M.U., Di Tommaso, P., and Nahnsen, S. (2020). The nf-core framework for community-curated bioinformatics pipelines. Nat Biotechnol *38*, 276–278. 10.1038/s41587-020-0439-x.

81. Amemiya, H.M., Kundaje, A., and Boyle, A.P. (2019). The ENCODE Blacklist: Identification of Problematic Regions of the Genome. Sci Rep *9*, 9354. 10.1038/s41598-019-45839-z.

82. O'Leary, N.A., Wright, M.W., Brister, J.R., Ciufo, S., Haddad, D., McVeigh, R., Rajput, B., Robbertse, B., Smith-White, B., Ako-Adjei, D., et al. (2016). Reference sequence (RefSeq) database at NCBI: current status, taxonomic expansion, and functional annotation. Nucleic Acids Res *44*, D733-745. 10.1093/nar/gkv1189.

83. Wright, G.W., and Simon, R.M. (2003). A random variance model for detection of differential gene expression in small microarray experiments. Bioinformatics *19*, 2448–2455. 10.1093/bioinformatics/btg345.

84. Picelli, S., Faridani, O.R., Björklund, Å.K., Winberg, G., Sagasser, S., and Sandberg, R. (2014). Full-length RNA-seq from single cells using Smart-seq2. Nature Protocols *9*, 171–181. 10.1038/nprot.2014.006.

85. Robinson, M.D., and Oshlack, A. (2010). A scaling normalization method for differential expression analysis of RNA-seq data. Genome Biology *11*, R25. 10.1186/gb-2010-11-3-r25.

86. Zuker, M. (2003). Mfold web server for nucleic acid folding and hybridization prediction. Nucleic Acids Research *31*, 3406–3415. 10.1093/nar/gkg595.

87. Bailey, T.L. (2021). STREME: accurate and versatile sequence motif discovery. Bioinformatics *37*, 2834–2840. 10.1093/bioinformatics/btab203.

88. Hon, J., Martínek, T., Zendulka, J., and Lexa, M. (2017). pqsfinder: an exhaustive and imperfection-tolerant search tool for potential quadruplex-forming sequences in R. Bioinformatics *33*, 3373–3379. 10.1093/bioinformatics/btx413.

89. Giudice, G., Sánchez-Cabo, F., Torroja, C., and Lara-Pezzi, E. (2016). ATtRACT—a database of RNA-binding proteins and associated motifs. Database *2016*, baw035. 10.1093/database/baw035.

90. Baird, T.D., Palam, L.R., Fusakio, M.E., Willy, J.A., Davis, C.M., McClintick, J.N., Anthony, T.G., and Wek, R.C. (2014). Selective mRNA translation during eIF2 phosphorylation induces expression of IBTKα. MBoC *25*, 1686–1697. 10.1091/mbc.e14-02-0704.

91. Larsson, O., Li, S., Issaenko, O.A., Avdulov, S., Peterson, M., Smith, K., Bitterman, P.B., and Polunovsky, V.A. (2007). Eukaryotic translation initiation factor 4E induced progression of primary human mammary epithelial cells along the cancer pathway is associated with targeted translational deregulation of oncogenic drivers and inhibitors. Cancer Res *67*, 6814–6824. 10.1158/0008-5472.CAN-07-0752.

92. Krokowski, D., Jobava, R., Szkop, K.J., Chen, C.-W., Fu, X., Venus, S., Guan, B.-J., Wu, J., Gao, Z., Banaszuk, W., et al. (2022). Stress-induced perturbations in intracellular amino acids reprogram mRNA translation in osmoadaptation independently of the ISR. Cell Rep *40*, 111092. 10.1016/j.celrep.2022.111092.

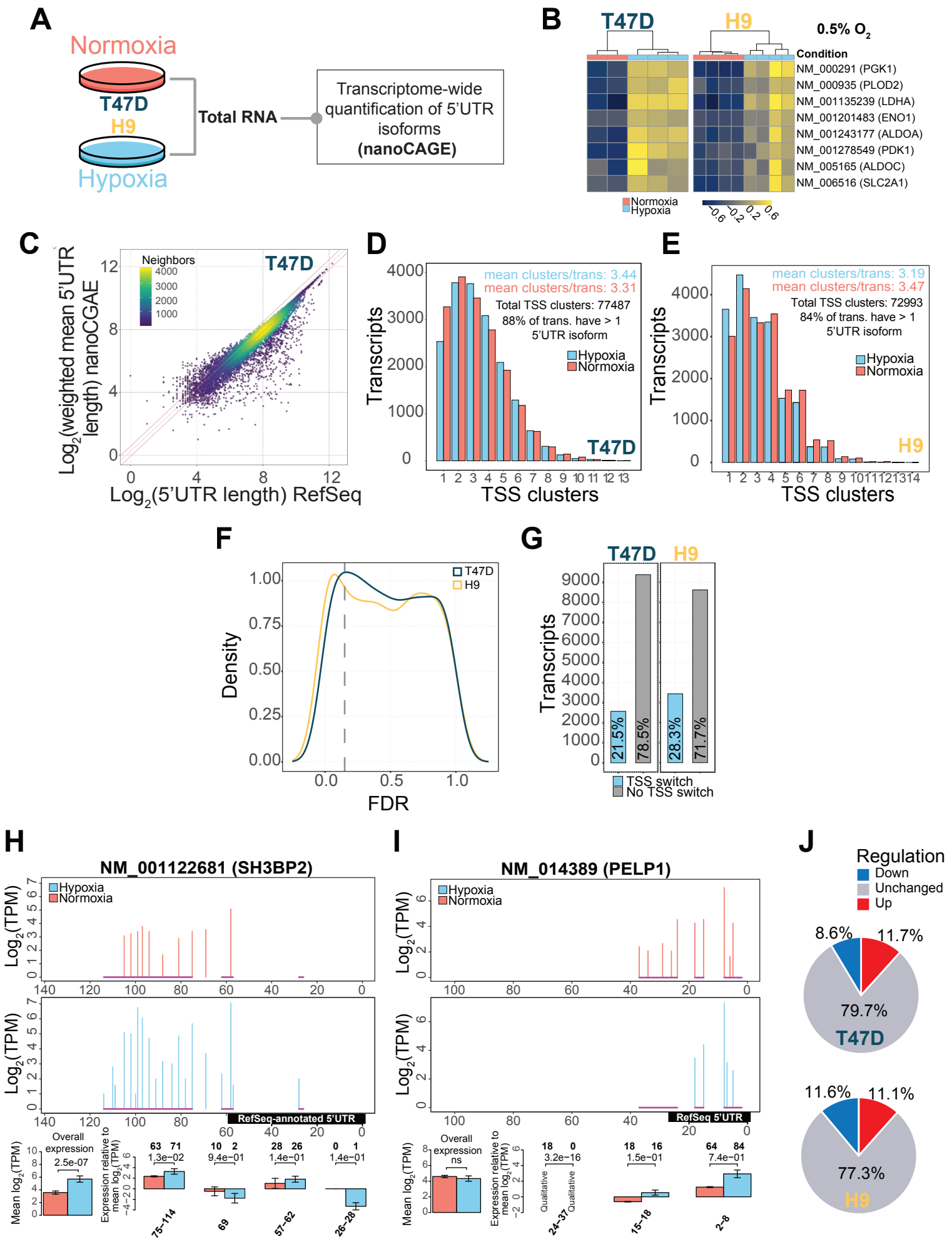

Figure 1; Watt *et al.*

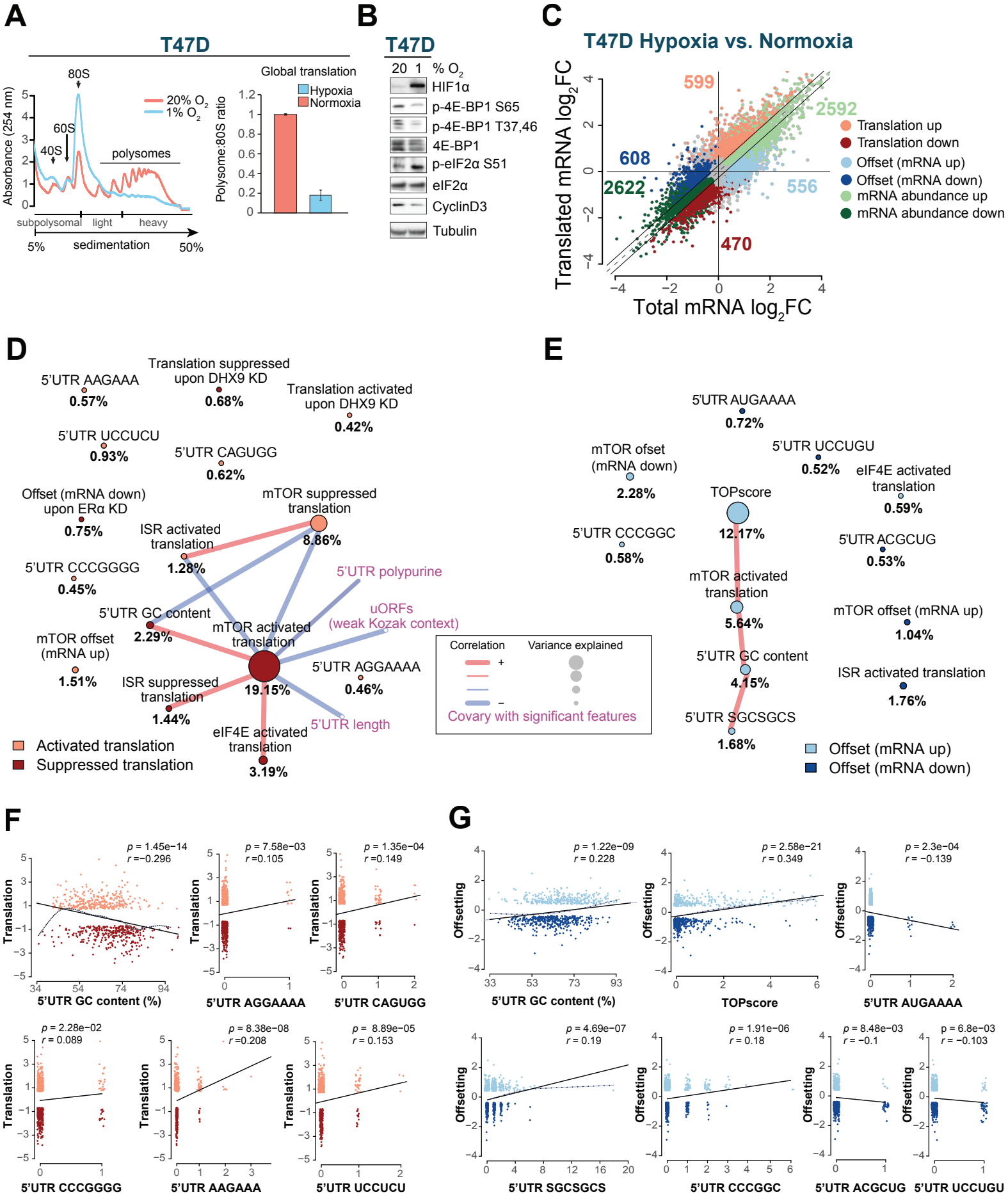

Figure 2; Watt *et al.*

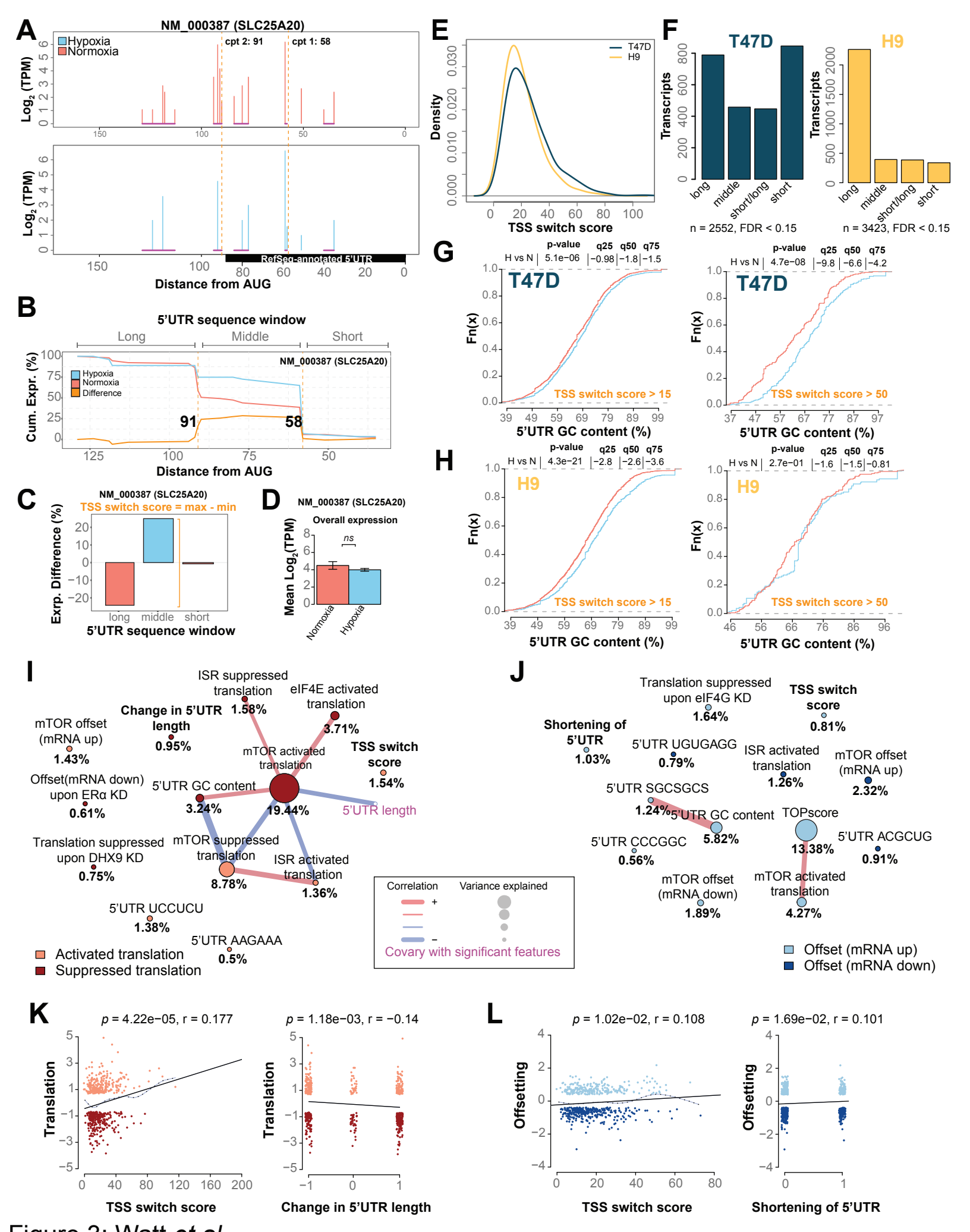

Figure 3; Watt *et al.*

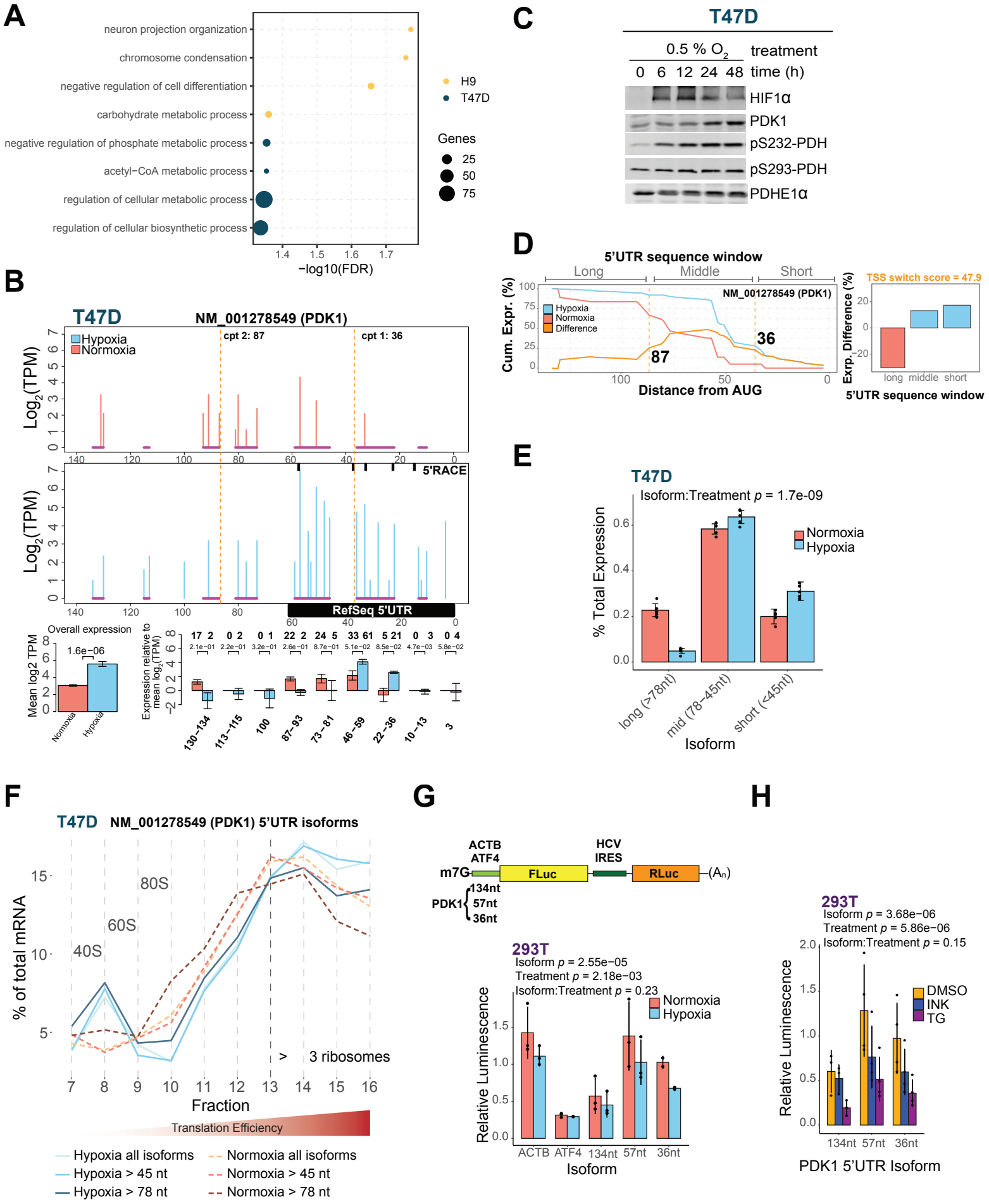

Figure 4; Watt *et al.*

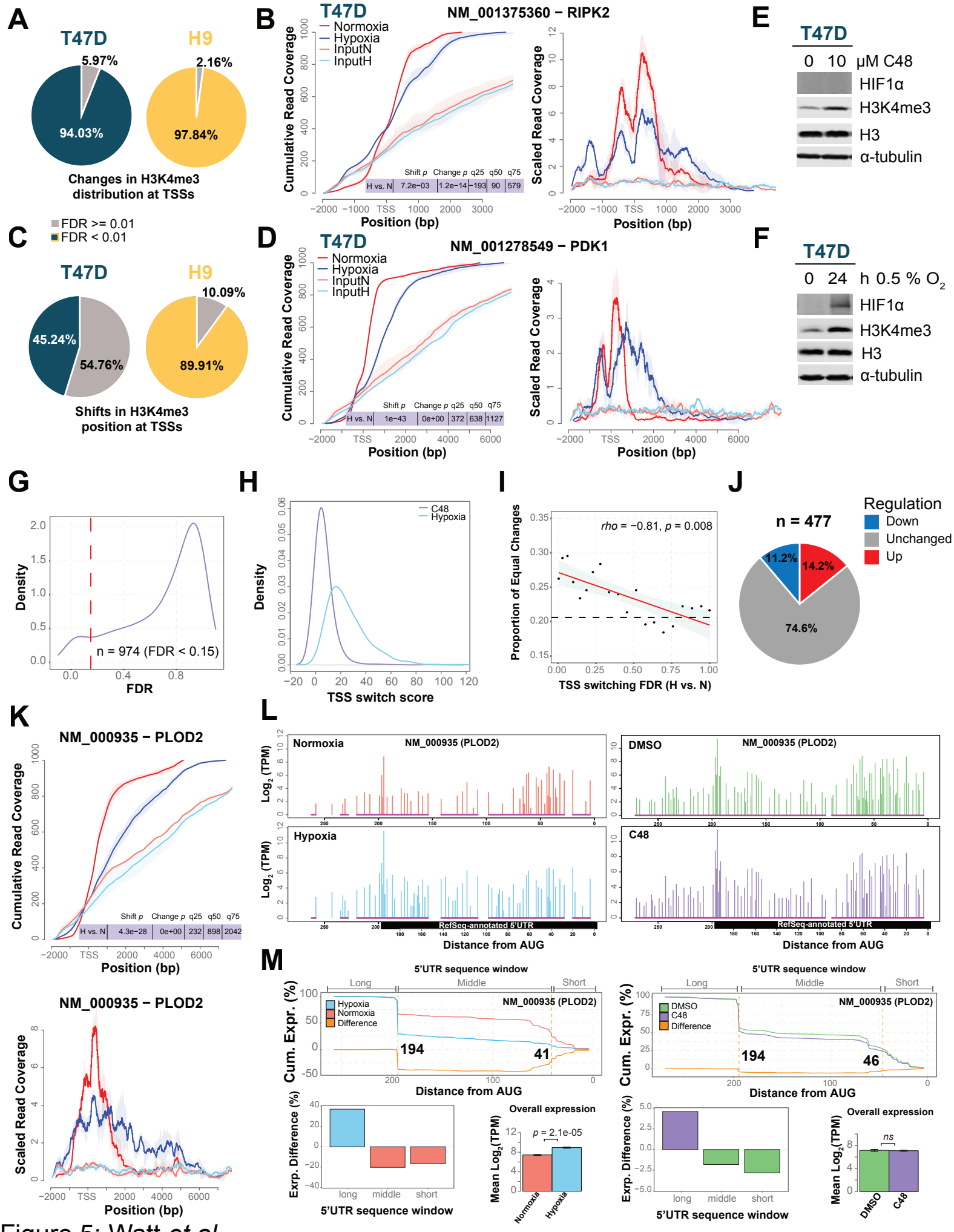

Figure 5; Watt *et al.*

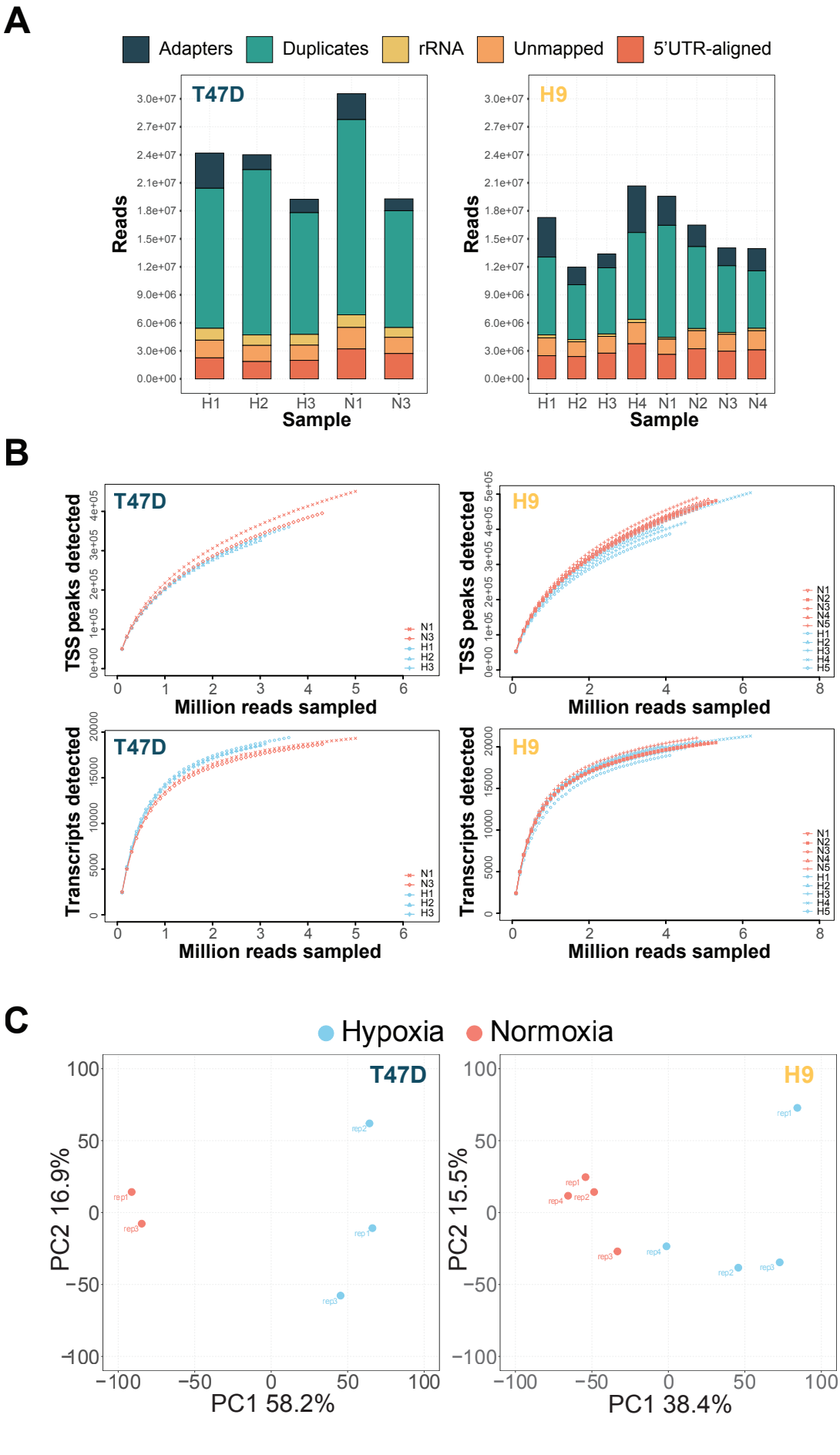

Figure S1; Watt *et al.*

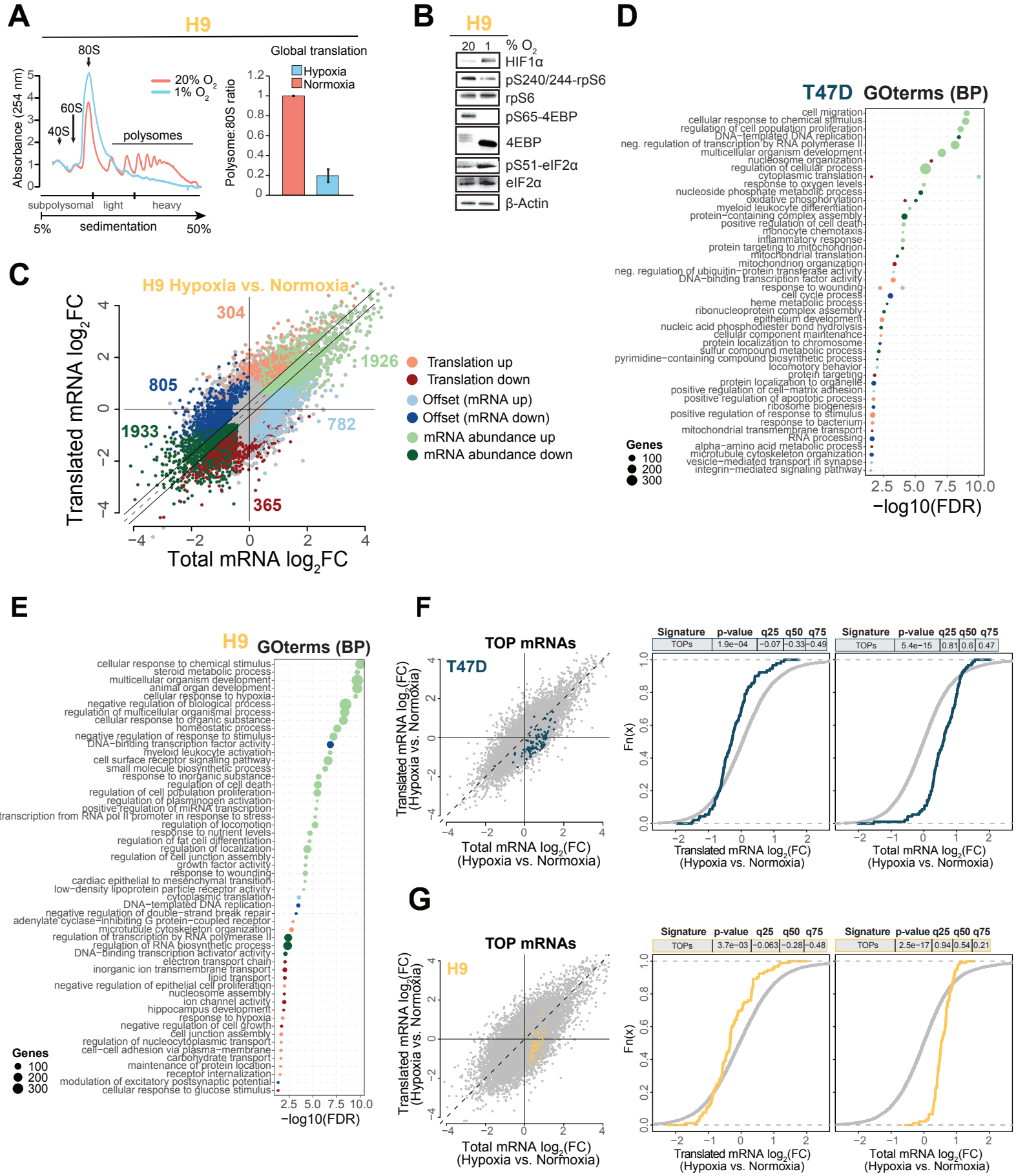

Figure S2; Watt *et al.*

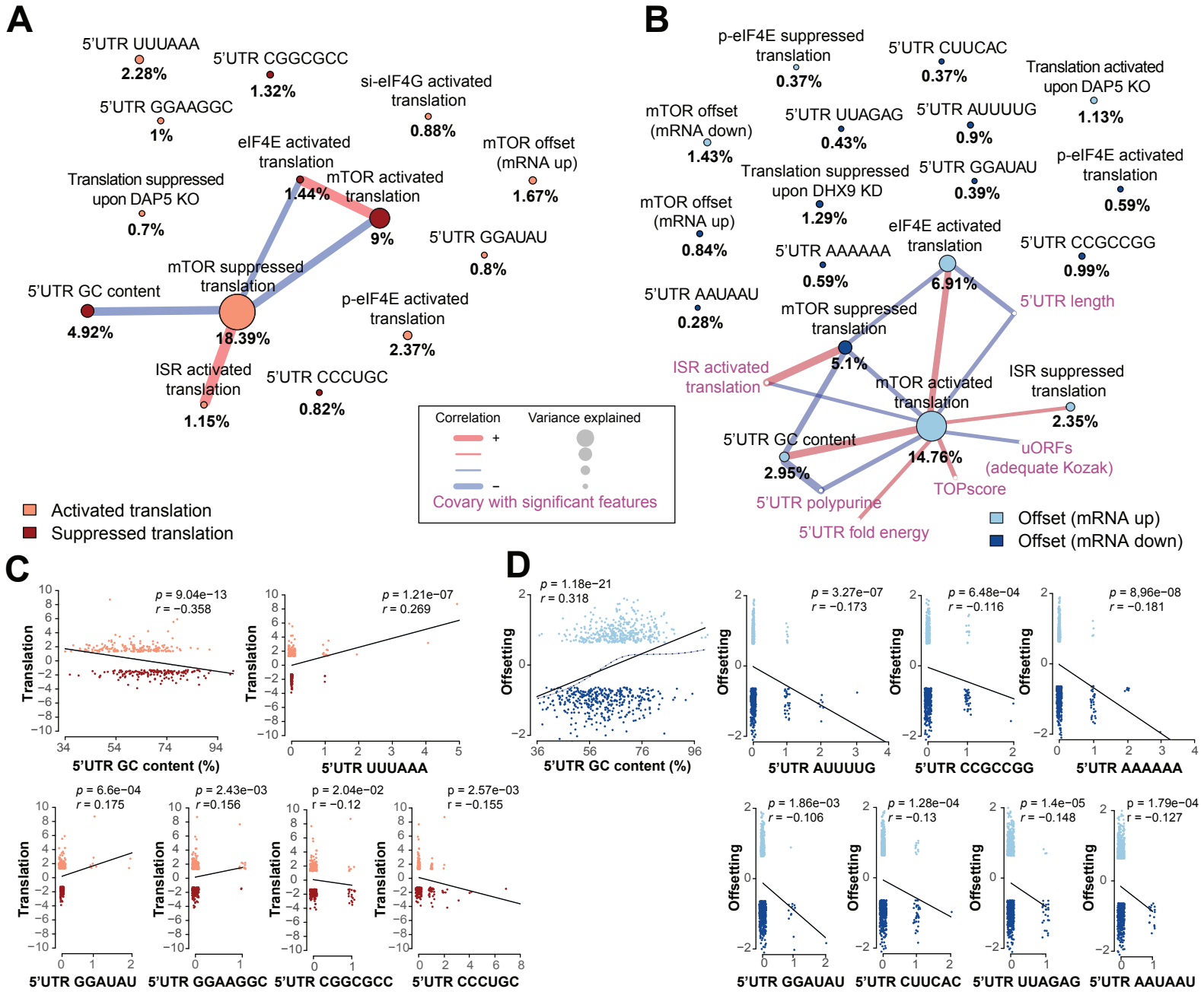

Figure S3; Watt *et al.*

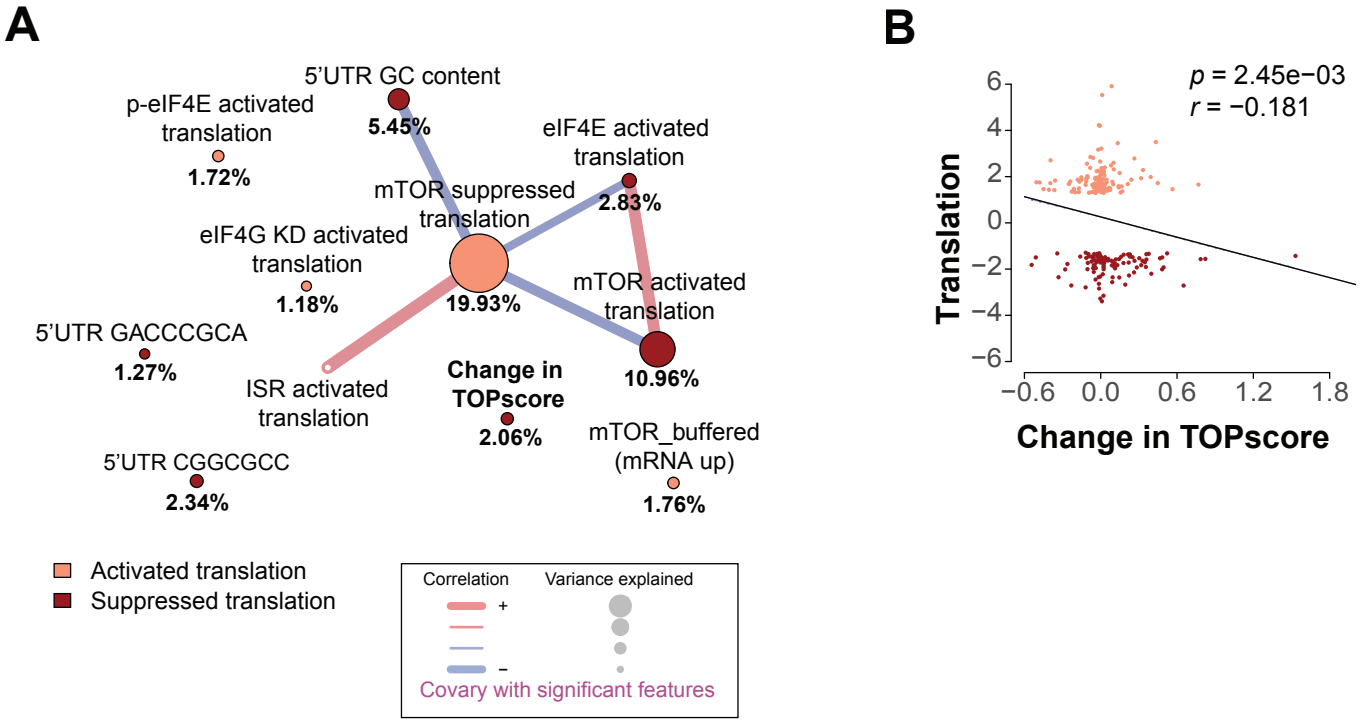

Figure S4; Watt *et al.*

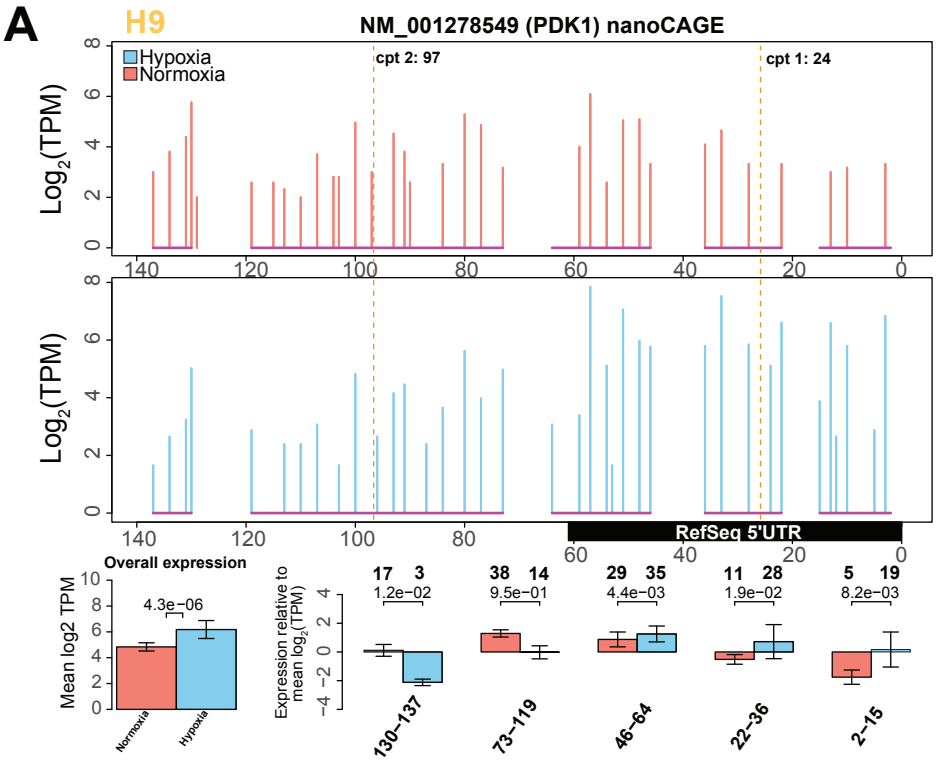

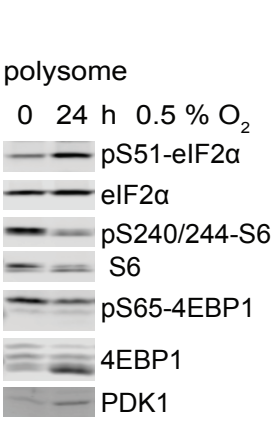

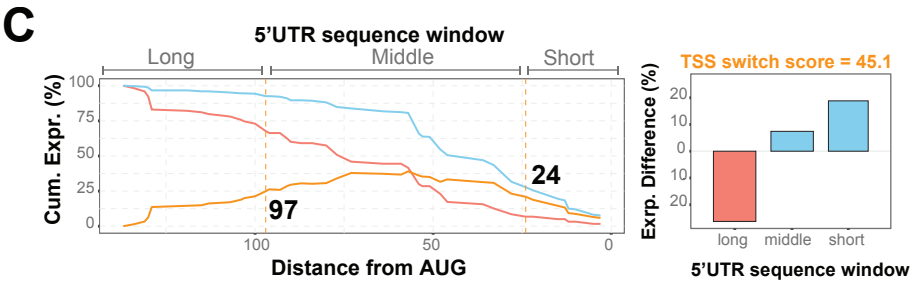

Figure S5; Watt *et al.*

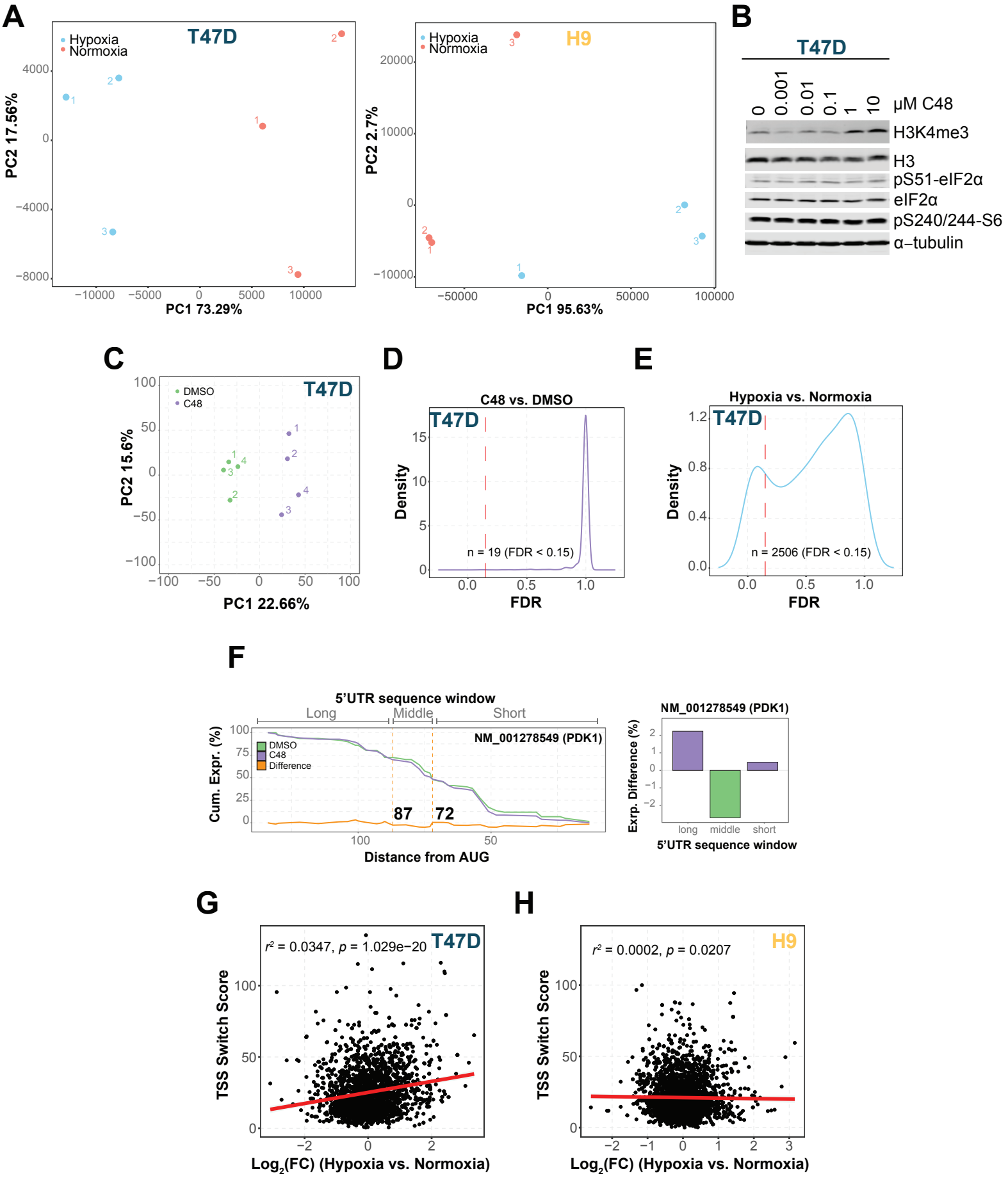

Figure S6; Watt *et al.*